Title: Glutamate release is inhibitory and unnecessary for the long-term potentiation of presynaptic function

Authors: Zahid Padamsey[1*], Rudi Tong[1], and Nigel Emptage[1*]

Affiliations: [1]University of Oxford, Department of Pharmacology, Mansfield Road, Oxford, OX1 3QT, UK

*Email: Zahid Padamsey (zahid.padamsey@pharm.ox.ac.uk) and Nigel Emptage (nigel.emptage@pharm.ox.ac.uk)

Keywords: hippocampus; Schaffer-collateral syanpses; synaptic plasticity; long-term potentiation; long-term depression; presynaptic plasticity; release probability; Ca^{2+} imaging; nitric oxide; L-type voltage-gated Ca^{2+} channels, NMDA receptor

Abstract

Long-term potentiation (LTP) and long-term depression (LTD) of transmitter release probability (P_r) are thought to be triggered by the activation of glutamate receptors. Here, we demonstrate that glutamate release at CA3-CA1 synapses is in fact inhibitory and unnecessary for increases in P_r. Instead, at active presynaptic terminals, postsynaptic depolarization alone can increase P_r by promoting the release of nitric oxide from neuronal dendrites in a manner dependent on L-type voltage-gated Ca^{2+} channels. The release of glutamate, in contrast, decreases P_r by activating presynaptic NMDA receptors (NMDAR). Thus, net changes in P_r are determined by the combined effect of both LTP-promoting and LTD-promoting processes, that is, by the amount of glutamate release and postsynaptic depolarization that accompany presynaptic activity, respectively. Neither of these processes directly depends on the activation of postsynaptic NMDARs. We further show that presynaptic changes can be captured by a simple mathematical framework, in which the role of presynaptic plasticity is to ensure that the ability for a presynaptic terminal to release glutamate is matched with its ability to predict postsynaptic spiking.

Introduction

Learning and memory are thought to require synaptic plasticity, which refers to the capacity for synaptic connections in the brain to change with experience. The most frequently studied forms of synaptic plasticity are long-term potentiation (LTP) and long-term depression (LTD), which involve long-lasting increases and decreases in synaptic transmission. LTP and LTD can be expressed either postsynaptically, as changes in AMPA receptor (AMPAR) number or presynaptically, as changes in glutamate release probability (P_r) [1-6]. Traditionally, postsynaptic NMDA receptor (NMDAR) activation is believed to be important for both pre- and post- synaptic forms of plasticity [2, 7]. Postsynaptic changes, in particular, have been causally and convincingly linked to NMDAR-dependent Ca^{2+} influx which, via the activation of postsynaptic Ca^{2+}-sensitive kinases and phosphatases, triggers changes in the number of synaptic AMPARs [7]. The link between NMDAR activation and presynaptic plasticity, however, is not as well studied. In the case of presynaptic LTP induction, it is traditionally thought that Ca^{2+} influx through postsynaptic NMDARs triggers the synthesis and release of a retrograde signal, most likely nitric oxide (NO), which in turn triggers increases in P_r [8, 9]. Several studies, however, have suggested that presynaptic enhancement can actually be induced in the presence of NMDAR antagonists. This form of plasticity relies on L-type voltage-gated Ca^{2+} channels (L-VGCCs) [10-14], but still depends on NO signalling [15]. These findings suggest that presynaptic plasticity requires neither the activation of NMDARs nor NMDAR-dependent NO synthesis.

Glutamate release is inevitably necessary to drive the postsynaptic depolarization required for LTP. This function of glutamate is not site-specific, since depolarization triggered by one synapse will spread to another. The necessity for site-specific release of glutamate in the induction of LTP is instead imposed by postsynaptic NMDARs, since NMDAR-mediated Ca^{2+} signalling is needed for the postsynaptic expression of LTP [2, 7] . Consequently, manipulations that enhance postsynaptic NMDAR signalling at the level of the single synapse reliably augment the induction of postsynaptic LTP [7, 16-18]. However,

that NMDARs are unlikely to be necessary for the induction of presynaptic LTP, suggests that the role of synapse-specific glutamate release in presynaptic plasticity may be different. Indeed, a common finding across a number of studies is that high P_r synapses are more likely to show presynaptic depression whereas low P_r synapses are more likely to show presynaptic potentiation [19-23]. Moreover, glutamate release is known to activate presynaptic NMDARs [24], which can induce presynaptic LTD [25]. Thus enhanced glutamate release at a presynaptic terminal, unlike as the dendritic spine, may not necessarily result in enhanced potentiation, but instead promote depression. Several studies have also demonstrated that presynaptic terminals initially releasing little or no glutamate are reliably potentiated following tetanic stimulation [19-24, 26, 27]. How low P_r synapses, including those that are putatively silent, can undergo such activity-dependent potentiation raises questions as to the exact role of glutamate in presynaptic plasticity.

Here we re-examined the mechanisms underlying activity-dependent presynaptic changes at CA3-CA1 hippocampal synapses, with a particular focus on understanding the role of glutamate in presynaptic plasticity. We bidirectionally manipulated glutamatergic signalling during synaptic activity and examined the resulting consequences on P_r at single synapses using Ca^{2+} imaging. Remarkably we found that site-specific glutamatergic signalling was unnecessary for the induction of presynaptic LTP. Postsynaptic depolarization alone could increase P_r at active presynaptic terminals by promoting the release of NO from neuronal dendrites in a manner dependent on L-VGCC activation. This increase was both Hebbian, in that it required presynaptic activity to precede postsynaptic depolarization, and site-specific, in that it did not spread to inactive terminals. Glutamate release, in contrast, promoted decreases in P_r by activating presynaptic NMDARs. Our findings support a simple mathematical model in which net changes in P_r at a presynaptic terminal depends on the amount of glutamate release and postsynaptic depolarization that accompanies presynaptic activity, suggesting that LTP-promoting processes and LTD-

promoting processes do not operate separately, but rather jointly to tune P_r at individual synapses.

Results

High frequency presynaptic activity inhibits presynaptic LTP and augments presynaptic LTD

We were interested in understanding the mechanisms underlying activity-dependent presynaptic changes at CA3-CA1 synapses, with a particular focus on understanding the role glutamate plays in presynaptic plasticity. We started by examining how manipulating glutamatergic signalling at synapses would affect activity-driven changes in presynaptic function. We recorded excitatory postsynaptic potentials (EPSPs) in CA1 neurons in hippocampal slice cultures. Cells were recorded using patch electrodes (4-8MΩ) and EPSPs were evoked by Schaffer-collateral stimulation. Baseline EPSP recordings were kept short ($\leq$ 5 minutes) to minimize postsynaptic dialysis which impedes LTP induction. Following baseline recording, we induced LTP by pairing presynaptic stimulation with postsynaptic depolarization. Pairings were causal, in that presynaptic stimuli preceded postsynaptic spiking by 7-10ms. A single pairing was repeated 60 times at 5Hz. For postsynaptic depolarization, we injected current of sufficient amplitude to generate 3-6 postsynaptic spikes over a 50ms time course, with the first spike starting 7-10ms following the start of current injection (see Figure 3A for example). Spikes often tended to broaden over the time course of injection. The resulting waveform resembled a complex spike, which is known to efficiently drive LTP *in vitro* [28-31] and has been recorded in the hippocampus *in vivo* [32, 33]. We found that this pairing protocol produced robust and reliable LTP (fold $\Delta EPSP_{slope}$: 1.88±0.24; n=6; p<0.01; Figure 1A,B), which had a presynaptic component of expression, as assessed by a decrease in the paired pulse ratio (PPR) (ΔPPR: -0.39±0.15; n=6; p<0.01; Figure 1C).

We next examined the effects of elevating glutamatergic signalling during LTP induction on presynaptic plasticity. Under physiological conditions, elevated glutamate signalling arises from increased presynaptic activity. We therefore repeated our LTP experiments, but during induction, in the place of single presynaptic pulses, we delivered short, high frequency bursts of presynaptic stimuli stimuli to drive more glutamate release. The burst consisted of two pulses, delivered 5ms apart, and resembled high-frequency bursting activity recorded in CA3 neurons *in vivo* [34]. We found that this protocol produced significantly less LTP compared to single pulse pairings (fold $\Delta EPSP_{slope}$: 1.36±0.13; n=6; vs. single pulse pairings: $p<0.05$), and was accompanied by no significant changes in PPR (ΔPPR: 0.00±0.04; n=6; $p>0.99$; Figure 1C), suggesting that LTP was likely to be expressed exclusively postsynaptically. These findings suggest that high frequency presynaptic activity can inhibit the induction of presynaptic LTP.

We repeated our experiments, but during LTP induction, we omitted postsynaptic depolarization (unpaired stimulation). As expected, when single presynaptic pulses were delivered (60 pulses at 5 Hz) during induction, we observed no significant change in EPSP (fold $\Delta EPSP_{slope}$: 0.93±0.10; n=5; $p=0.11$; Figure 1D,E) or PPR (fold ΔPPR: 0.01±0.09; n=5; $p>0.99$; Figure 1F). However, when high frequency bursts were delivered during induction, we observed a robust decrease in the EPSP (fold $\Delta EPSP_{slope}$: 0.42±0.08; n=8; vs. single pairing: $p<0.01$; Figure 1D,E) and an increase in PPR (fold ΔPPR: 0.36±0.04; n=8; vs. single pulse pairing: $p<0.01$; Figure 1F), suggesting that we had induced LTD with a presynaptic component of expression. Collectively, these findings showed that high frequency presynaptic stimulation not only inhibited the induction of presynaptic LTP, but also promoted the induction of presynaptic LTD.

Glutamate photolysis inhibits presynaptic LTP and augments presynaptic LTD

We next tested whether the effects of high frequency presynaptic stimulation on presynaptic plasticity were in fact due to the presynaptic terminal releasing more glutamate, as opposed to other effects, such as an increased Ca^{2+} influx in the presynaptic

terminal. To do so, we opted to use glutamate uncaging, which would enable us to elevate glutamate release at synapses during LTP induction whilst keeping the frequency of presynaptic stimulation constant. To keep the experiment as physiological as possible, we restricted glutamate uncaging to single synapses. We then monitored activity-dependent changes in P_r at these synapses by imaging postsynaptic Ca^{2+} transients, as previously described [27, 35]. This technique relies on the fact that at most CA3-CA1 synapses, uniquantal glutamate release, through AMPAR-mediated depolarization, generates sufficient Ca^{2+} influx from NMDAR and voltage-gated Ca^{2+} channels (VGCCs) to be detected by Ca^{2+}-sensitive dyes [1, 36, 37]. Consequently, the proportion of trials in which single presynaptic stimuli generate postsynaptic Ca^{2+} transients can be used to calculate P_r at single synapses [37].

CA1 pyramidal neurons were loaded with the Ca^{2+} sensitive dye Oregon Green BAPTA-1, and a fluorescently-labelled glass electrode was used stimulate Schaffer-collaterals in the vicinity of the imaged dendrite (Figure 2A). Dendritic spine fluorescence was examined in order to identify synapses that were responsive to stimulation. To increase the likelihood of visually identifying responsive synapses, especially those with low basal release probabilities, we always delivered two presynaptic stimuli, 70ms apart, to transiently increase P_r (Figure 2B). When a synapse was found that responded to stimulation, it always responded in an all-or-none manner, with Ca^{2+} transients largely restricted to the spine head. As expected, Ca^{2+} transients were also more likely to be elicited by the second of the two presynaptic stimuli because of the effects of short-term plasticity. P_r was calculated as the proportion of trials in which the first of the two presynaptic stimuli generated a fluorescent increase in the spine head; the second of the two presynaptic stimuli was ignored.

Because of the additional time requirements of these experiments, cells were recorded from using sharp microelectrodes (80-120MΩ) to minimize dialysis that otherwise compromises LTP induction. Following baseline measurements of P_r, we induced LTP as

before, by delivering 60 individual presynaptic stimuli at 5Hz, each paired with postsynaptic depolarization Consistent with our electrophysiological results, this protocol evoked an increase in P_r (ΔP_r: 0.19±0.03; n=14; Figure 2B,D,F) and a long-lasting potentiation of the recorded EPSP (fold $\Delta EPSP_{slope}$:1.97±0.13; n=12; Figure 2G,I). We then repeated the experiment but this time, during LTP induction, each presynaptic stimulus was paired with photolysis of caged glutamate at the synapse. We adjusted the laser power to ensure that photolysis mimicked the fluorescent changes elicited by uniquantal glutamate release evoked by electrical stimulation ($\Delta F/F$ photolysis vs. stimulation: 0.38±0.08 vs. 0.43±0.09; n=12; p=0.72; Figure 2A). Remarkably, under these conditions, increases in P_r at the target synapse were effectively abolished (ΔP_r: -0.02±0.03; n=12; photolysis vs. control: $p < 0.001$; Figure2B,D,F). This demonstrates that, consistent with our hypothesis, elevated glutamatergic signalling at synapses inhibited the induction of presynaptic LTP. Notably, in these experiments, LTP induction did result in a similar enhancement of the EPSP as in control experiments (fold $\Delta EPSP_{slope}$: 2.06±0.20; n=11; photolysis vs. control: p=0.48; Figure 2G,I), suggesting that the failure for the imaged synapse to support LTP could not be attributed to the failure of the recorded cell or slice to support LTP. In five experiments, LTP induction was repeated for a second time at the same synapse, in the absence of caged glutamate, but with photolytic laser exposure; under these conditions, the expected increase in P_r was observed (ΔP_r: 0.18±0.02; n=5; post-photolysis control in Figure 2D). Increases in P_r were also observed in control experiments, in which LTP induction was conducted in the presence of caged glutamate, but in the absence of photolytic laser exposure (ΔP_r: 0.21±0.08; n=3). These results suggest that the inhibitory effect of photolysis on P_r was due to glutamate release, as opposed to non-specific effects of uncaging.

We also examined the effects of glutamate photolysis delivered in the absence of postsynaptic depolarization (unpaired stimulation). Delivery of 60 presynaptic stimuli at 5 Hz, as before, had no effect on the recorded EPSP (fold $\Delta EPSP_{slope}$: 1.03±0.10; n=9; p>0.99; Figure 2H,I), consistent with our previous result, and produced no changes in P_r at the

majority of synapses imaged (Figure 2C,E,F). We did, however, notice that synapses with initially high release probabilities (Pr>0.5), showed a modest decrease in P_r following unpaired stimulation (Figure 2E); this decrease was not likely to be detected by electrophysiological recordings because high P_r synapses comprise an estimated <10% of synapses in our preparation [35]. Remarkably, when we coupled each presynaptic stimulus with glutamate photolysis, we now observed decreases in P_r at all imaged synapses, regardless of their initial P_r (ΔP_r photolysis vs. control: -0.33±0.08 vs. -0.12±0.06; n=9,10 p=0.037; Figure 2C,E,F). Consistent with our hypothesis, these findings suggest that elevated glutamate release at a synapse inhibited presynaptic LTP and, in the absence of postsynaptic depolarization, drove presynaptic LTD.

Presynaptic LTP can be induced in complete glutamate receptor blockade

Given that augmenting glutamatergic signalling inhibited the induction of presynaptic LTP, we asked if glutamate release was required at all for driving increases in P_r during paired stimulation. We reasoned that although the activation of glutamate receptors would ultimately be necessary to drive the postsynaptic depolarization required for LTP induction, presynaptic potentiation may not actually require any one presynaptic terminal to trigger glutamate release, provided that its activity coincides with postsynaptic depolarization, which could be triggered by glutamate release at other co-active synapses.

To test this possibility we attempted to induce LTP at CA3-CA1 synapses in hippocampal slices with all known glutamate receptors (AMPARs, KainateRs, NMDARs, and mGluRs) pharmacologically inhibited (10µM NBQX, 50-100µM AP5, 0.5-1mM MCPG, 100µM LY341495). Given the additional time requirements for these experiments, we recorded from CA1 neurons using high-resistance patch electrodes (18-25MΩ) to limit postsynaptic dialysis. Following abolishment of the EPSP, synaptic activity was causally paired as before with complex spikes (Figure 3A). The antagonist cocktail was washed out, and the EPSP was allowed to recover. As expected, drug washout was never complete (Figure 3C,D) and so it was necessary to compare the EPSP recorded from the pathway receiving paired

stimulation to a second, independent control pathway recorded simultaneously (Figure 3A,B). We found that pairing induced a robust enhancement of the EPSP in the stimulated pathway (fold $\Delta EPSP_{slope}$ paired vs. control: 1.12±0.13vs. 0.71±0.12; n = 7; $p < 0.05$; Figure 3B,D), which lasted for the duration of the recording (up to 40-90 minutes post-pairing). Pairing resulted in a 1.72±0.21 fold potentiation ($p<0.05$), which we estimated by normalizing the fold change in the EPSP of the paired pathway to that of the control pathway. Notably, EPSP recovery of the control pathway was not significantly different from experiments in which drugs were applied in the absence of paired stimulation (control vs. drugs-only: 0.71±0.12 vs. 0.54±0.11; n = 7 and 5; p = 0.33; Figure 3C,D), suggesting that LTP was restricted to only synapses that were active during the pairing.

We next examined the locus of LTP expression. We found that LTP induction in glutamate receptor blockade was accompanied by a significant increase in the co-efficient of variation parameter (CV^{-2}) (paired vs. control: 2.80 ±0.79 vs. 0.89 ±0.10; n = 7; $p<0.01$; Figure 3E), and a significant decrease in PPR (paired vs. control ΔPPR: -0.28±0.06 vs. 0.03±0.03; n = 6; $p<0.01$; Figure 3F). Both of these changes are consistent with a presynaptic component of LTP expression, and both were found only in the paired pathway, suggesting that LTP induction was site-specific.

We also confirmed that presynaptic enhancements could be induced under glutamate receptor blockade in acute hippocampal slices ($\Delta EPSP_{slope}$ paired vs. control: 0.65 ±0.18 vs. 0.43±0.14; n = 6; $p<0.05$; Supplemental Figure 1 and 2). Pairing resulted in a 1.56±0.11 fold potentiation ($p<0.01$), which we again estimated by normalizing the fold change in the EPSP of the paired pathway to that of the control pathway. As with slice cultures, these enhancements were accompanied by significant decreases in the PPR (ΔPPR stimulated vs. control: -0.23±0.07 vs. 0.04±0.04; n = 6; $p<0.01$), and by significant increases in CV^{-2} (fold ΔCV^{-2} stimulated vs. control: 1.73 ±0.20 vs. 0.87±0.13; n = 6; $p<0.01$) (Supplemental Figure 1 and 2) that were only evident in the paired pathway, suggesting that the changes were both presynaptic in origin and site-specific.

LTP induction in glutamate receptor blockade is associated with an increase in P_r

We then returned to Ca^{2+} imaging to determine whether we could directly observe increases in P_r at single synapses associated with the induction of LTP in glutamate receptor blockade (Figure 4). To minimise dialysis for these experiments during drug wash-in, imaging was conducted in the absence of electrophysiological recordings on CA1 neurons that were pre-loaded with Ca^{2+} indicator dye (see Methods). Following an initial assessment of P_r, glutamate receptor antagonists (APV, NBQX, MCPG, and LY341495) were bath applied and the imaged cell was transiently patched in order to drive postsynaptic depolarization during paired stimulation. Consistent with electrophysiological findings, causal pairing of pre- and post- synaptic depolarization produced robust and reliable increases in P_r (ΔP_r: 0.40±0.06; n=7; Figure 4A-C). No such changes were elicited by drug application in the absence of pairing (ΔP_r: 0.04±0.04; n=7; vs. causal pairing: $p<0.01$), or by either presynaptic stimulation alone (ΔP_r: -0.03±0.03; n=7; vs. causal pairing: $p<0.01$) or postsynaptic stimulation alone (ΔP_r: -0.01±0.04; n=6; vs. causal pairing: $p<0.01$), or when postsynaptic depolarization preceded, rather than followed, presynaptic stimulation during pairing (ΔP_r: -0.02±0.06; n=6; vs. causal pairing: $p<0.01$) (Figure 4B,C). The induction of presynaptic LTP in the absence of glutamatergic signalling was therefore Hebbian, requiring presynaptic activity to be causally paired with strong postsynaptic depolarization.

Postsynaptic depolarization increases P_r by promoting dendritic release of nitric oxide in a manner dependent on L-type voltage-gated Ca^{2+} channels

We next investigated the mechanism by which paired stimulation could trigger increases in P_r in the absence of glutamatergic signalling. The requirement for postsynaptic depolarization in the induction of presynaptic potentiation suggests a need for a diffusible retrograde messenger. Perhaps the most promising, albeit still controversial, retrograde signal implicated in LTP induction is nitric oxide (NO) [14]. Although NO synthesis has classically been associated with the activation of postsynaptic NMDARs [9], there is some

suggestion that Ca^{2+} influx from L-type voltage-gated Ca^{2+} channels (L-VGCCs), which have previously been implicated in presynaptic LTP [12, 13, 15], may also trigger NO production [15, 38, 39]. If NO synthesis in neuronal dendrites can be triggered by L-VGCC activation, then NO production could occur in a manner dependent on postsynaptic depolarization, but independent of glutamatergic signalling. To test this hypothesis, we first asked whether presynaptic LTP, induced in glutamate receptor blockade, was dependent on L-VGCC activation and NO signalling. Consistent with our hypothesis, we found that pairing-induced increases in P_r (ΔP_r: 0.34±0.04; n = 10; $p<0.01$) were reliably abolished by bath application of the L-VGCC antagonist nitrendipine (ΔP_r: 0.04±0.04; n=6; vs. blockade: $p<0.01$) and by the NO scavenger carboxy-PTIO (cPTIO), either bath applied (ΔP_r: -0.02±0.04; n=7; vs. blockade: $p<0.01$) or injected into the postsynaptic neuron (ΔP_r: -0.02±0.07; n=6; vs. blockade: $p<0.01$) (Figure 5A). Nitrendipine and cPTIO similarly blocked presynaptic enhancements induced under glutamate receptor blockade in acute hippocampal slices (Supplemental Figure 1 and 2), suggesting that, as in cultured slices, presynaptic efficacy in acute slices was similarly regulated by NO signalling.

We then examined whether NO production depended on L-VGCC activation. We transiently patched CA1 neurons in order to load them with the NO-sensitive dye, DAF-FM, and then measured fluorescent changes in the apical dendrites prior to and following postsynaptic depolarization in glutamate receptor blockade. Given the poor signal-to-noise ratio associated with DAF-FM imaging, and to circumvent the problem of intracellular dialysis, we non-invasively evoked strong postsynaptic depolarization by elevating extracellular K^+, as previously described [38, 39]. Under these conditions, we observed robust fluorescent increases in neuronal dendrites ($\Delta F/F$: 0.38±0.04; n=5) (Figure 5B,C). These increases were dependent on NO synthesis as they could be prevented by postsynaptic injection of cPTIO ($\Delta F/F$: -0.03±0.05; n=5; vs. control: $p<0.01$) or bath application of the NO synthase (NOS) inhibitor L-NAME ($\Delta F/F$: 0.00±0.05; n=5; vs. control: $p<0.01$). Importantly, fluorescent increases were reliably abolished with nitrendipine

(ΔF/F: -0.02±0.06; n=5; vs. control: p<0.01) (Figure 5B,C), suggesting that NO synthesis required L-VGCC activation.

To then examine whether NO release alone was sufficient for the induction of presynaptic LTP, we examined whether increases in P_r could be elicited when presynaptic stimulation was paired with NO release, in the absence of postsynaptic depolarization. We paired 30-60 presynaptic stimuli, delivered at 5Hz in glutamate receptor blockade, with brief photolysis of caged NO (0.5-1mM $RuNOCl_3$) at the imaged synapse. Pairing was causal, with each NO photolysis event timed to occur 7-10ms after each presynaptic stimulus. Under these conditions, we found significant increases in P_r when assessed 30 minutes post-pairing (ΔP_r: 0.29±0.07; n=10; p<0.01; Figure 5D-F). No such changes were produced when pairing occurred in the presence of bath-applied cPTIO (ΔP_r: 0.02±0.07; n=6; vs. causal pairing: p<0.05; Figure 5E,F), suggesting that LTP did not result from non-specific effects associated with photolysis. Moreover, when presynaptic stimuli followed NO photolysis no significant change in P_r was observed (ΔP_r: -0.01±0.04; n=8; vs. causal pairing: p<0.01; Figure 5D-F), suggesting that NO-mediated potentiation was Hebbian, requiring presynaptic activity to precede, rather than follow, NO release.

Glutamate release decreases P_r via activation of presynaptic NMDARs

If glutamatergic signalling at a presynaptic terminal is not required for its potentiation, then what is the role of glutamate release in presynaptic plasticity? To investigate this we compared changes in P_r produced by activity in the presence and absence of glutamate receptor blockade. Remarkably, we found glutamate receptor blockade augmented increases in P_r produced by paired stimulation (ΔP_r blockade vs. control: 0.34±0.04 vs. 0.18±0.02; n = 10; p < 0.05; Figure 6A-C) and abolished decreases in P_r generated by unpaired stimulation (ΔP_r blockade vs. control: 0.00±0.03 vs. -0.21±0.05; n=10, 9; p<0.01; Figure 6D,E). These results suggest that glutamate release during synaptic activity promotes decreases in Pr, regardless of the accompanying levels of postsynaptic depolarization.

How might glutamate release depress P_r? We have previously reported that presynaptic NMDARs are found at CA3-CA1 synapses; these receptors act as reliable detectors for uniquantal glutamate release [24] and, at neocortical synapses, have been implicated in presynaptic LTD [40-43]. We therefore examined whether these receptors mediated the inhibitory effects of glutamate observed on presynaptic function.

Given the difficulties associated with selectively blocking pre-, as opposed to post-, synaptic NMDARs, several groups have investigated the role of presynaptic NMDARs in plasticity by comparing the effects of bath application of AP5 or MK801, which blocks both pre- and post- synaptic NMDARs, with that of intracellular MK801 application, which selectively blocks postsynaptic NMDARs [43-46]. We sought to use a similar approach. However, because MK801 does not readily washout, and since postsynaptic NMDARs greatly contribute to spine Ca^{2+} influx [36, 37, 47], we first examined whether the permanent loss of postsynaptic NMDAR signalling affected our ability to measure P_r using postsynaptic Ca^{2+} imaging. We found that at about 50% of synapses, NMDAR blockade reduced, but did not entirely abolish synaptically-evoked Ca^{2+} transients (Supplemental Figure 3). The residual Ca^{2+} transients were mediated by activation of voltage-gated Ca^{2+} channels (VGCCs) in response to AMPAR-mediated depolarization, and could be used to accurately measure P_r (Supplemental Figure 3). Importantly, the average P_r of these synapses did not significantly differ from that of synapses lacking a residual Ca^{2+} transient in NMDAR blockade (ΔP_r: AP5-sensitive vs. AP5-insensitive: 0.42=0.07 vs. 0.47=0.11; p=0.67; Supplemental Figure 3). These findings suggest that, in NMDAR receptor blockade, VGCC-dependent spine-Ca^{2+} influx can be used as a means of calculating P_r at a sizeable and representative proportion of presynaptic terminals.

Using VGCC-dependent spine Ca^{2+} transients, we found that when both pre- and post-synaptic NMDARs were blocked by bath application of either AP5 (n=9) or MK-801 (n=9), paired stimulation induced increases in P_r (ΔP_r: 0.34±0.03; n=18) that were not significantly different from those produced in full glutamate receptor blockade (p=0.77),

but that were greater than increases produced under control conditions ($p<0.01$) (Figure 6A-C). Bath application of AP5 or MK801, like full receptor blockade, also blocked decreases in P_r produced by unpaired stimulation (ΔP_r: -0.02±0.02; n=17; vs. blockade: p=0.53; Figure 6D,E). In contrast, with intracellular application of MK-801, which specifically blocked postsynaptic NMDARs, increases in P_r produced by paired stimulation (ΔP_r: 0.16±0.04; n=9; vs. control: p=0.84; Figure 6A-C) and decreases in P_r produced by unpaired stimulation (ΔP_r: -0.25±0.07; n=9; vs. control: p=0.90; Figure 6D,E) did not significantly differ from control conditions. These results were not attributable to an incomplete blockade of postsynaptic NMDARs by intracellular MK801 since the amplitude of spine Ca^{2+} transients under these conditions were not significantly different from those recorded in AP5 (ΔF/F: intracellular MK-801 vs. AP5: 0.32±0.05 vs.0.26±0.03 n=10 and 12; p=0.65), but were significantly smaller than those recorded in control conditions (ΔF/F: intracellular MK-801 vs. control: 0.32±0.05 vs.0.72±0.01; n=10 and 9; $p < 0.01$; Supplemental Figure 3). Collectively, these results suggest that pre-, but not post-, synaptic NMDARs mediate the inhibitory effect of glutamate release on P_r that is present in both LTP and LTD induction paradigms.

The inhibitory effect of presynaptic NMDARs on P_r would explain why glutamate photolysis in our earlier experiments (Figure 2) inhibited presynaptic LTP and promoted presynaptic LTD. To confirm this, we repeated photolysis experiments in the presence of MK-801, either intracellularly or extracellularly applied, again to differentially block presynaptic and postsynaptic NMDAR signalling (Figure 7). Consistent with our hypothesis, we found that bath, but not intracellular, application of MK-801 rescued LTP induction, despite the presence of uncaged glutamate at the synapse during postsynaptic depolarization (ΔP_r: bath MK-801 vs. photolysis: 0.37±0.05; vs. -0.02±0.02 n=7 vs 12; $p<0.01$; intracellular MK-801: -0.02±0.04; n=7; vs. photolysis: p=0.97; Figure 7A,B). Incidentally, increases in P_r were not only rescued by bath application of MK-801 but were significantly greater than in control conditions (ΔP_r control: 0.20±0.03; n=12; vs. bath MK-801: $p<0.05$; Figure 7A,B). This is likely because bath application of MK-801, in addition to

blocking the inhibitory effects of caged glutamate, additionally blocked the inhibitory effect of endogenous glutamate release that was present in control conditions (Figure 6B,C). As expected, bath, but not intracellular, application of MK-801 also prevented photolysis-induced augmentation of LTD, in which stimuli were delivered in the absence of postsynaptic depolarization (ΔP_r: bath MK-801 vs. photolysis: -0.02±0.03; vs. -0.29±0.06; n=7 vs 9; $p<0.01$; intracellular MK-801: -0.28±0.08; n=7; vs. photolysis: $p=0.92$; Figure 7C,D). Bath MK-801 application additionally prevented LTD induction present at high P_r synapses under control condition (Figure 7C,D) again, likely by blocking the inhibitory effects of endogenous glutamate release (Figure 6D,E).

A simple mathematical framework predicts activity-dependent changes in P_r

Our findings thus far suggest that changes in P_r are driven by two processes: 1) postsynaptic depolarization, which promotes increases in P_r through L-VGCC-dependent release of NO from neuronal dendrites, and 2) glutamate release, which promotes decreases in P_r through presynaptic NMDAR activation (Figure 8A). We have demonstrated that net changes in P_r will depend on both processes. This suggests that changes in P_r at a presynaptic terminal are driven by a *mismatch* between 1) the amount of postsynaptic depolarization and 2) the amount of glutamate release that accompanies presynaptic activity. We therefore asked whether these two variables could be incorporated into a mathematical framework that could predict change in P_r (ΔP_r) in our data set. For ease of calculation, we chose to quantify both these variables in terms of probabilities, that is, 1) the probability that presynaptic activity was accompanied by strong postsynaptic depolarization (P_{depol}) and 2) the probability that glutamate was released at the synapse (P_{glu}). The simplest mathematical framework to model changes in P_r would be: $\Delta P_r = \eta (P_{depol}-P_{glu})$, where net changes in P_r would be proportional to the relative difference or *mismatch* between P_{depol} and P_{glu} as defined by $(P_{depol}-P_{glu})$, multiplied by some constant η, defined as the learning rate (Figure 8B).

We applied the model $\Delta P_r = \eta(P_{depol}-P_{glu})$ to our data set of imaged synapses across all experimental conditions. As a reminder, to induce plasticity we had delivered 60 presynaptic stimuli at 5Hz, where each stimulus was either consistently paired or unpaired with postsynaptic depolarization. For conditions with paired stimulation, we set P_{depol} to 1, since depolarization was present for every presynaptic stimulus. However, for conditions in which NO signalling was inhibited, P_{depol} was set to 0, as the effects of depolarization would be absent for every presynaptic stimulus. For all other conditions, in which presynaptic stimuli were not paired with presynaptic stimulation, we set P_{depol} to 0. We then determined values for P_{glu}. For experiments involving glutamate photolysis, P_{glu} was set to 1, as glutamate was available for every presynaptic stimulus. For experiments in which presynaptic NMDARs were inhibited, P_{glu} was set to 0, as the inhibitory effects of glutamate were absent for every presynaptic stimulus. For all other conditions, P_{glu} had to be calculated for each synapse. Although P_{glu} will likely be proportional to the initial P_r of a synapse, it will not be equivalent to initial P_r owing to short-term plasticity effects induced during the 5Hz stimulation train [24]. To obtain a more accurate estimate of P_{glu}, we conducted an additional set of experiments, in which we used Ca^{2+} imaging to examine glutamate release at single synapses stimulated with 60 presynaptic pulses delivered at 5Hz (Supplemental Figure 4). We calculated P_{glu} as the total number of glutamate release events in the train divided by the number of pulses in the train (i.e. 60). When plotted against initial P_r, we obtained a linear relationship with which to relate P_{glu} to initial P_r (P_{glu} = 0.475*initial P_r + 0.2175; Supplemental Figure 4). We used this relationship to derive estimates of P_{glu} for synapses in the remainder of our data set. Finally, we determined the learning rate η, which obtained the best fit of the model (η=0.35).

To assess the goodness of fit of our model, we divided the remainder of our data (n=216 synapses) into 6 categories, depending on whether the effects of postsynaptic depolarization were present or absent, whether glutamate photolysis was present or absent, and whether presynaptic NMDAR blockade was present or absent. These 6

categories, along with the models predictions for ΔP_r are shown in Figure 8C and are summarized in the table below.

No.	Effects present	P_{depol}	P_{glu}	$\Delta P_r = \eta (P_{depol}-P_{glu})$
1	Paired stimulation + photolysis	1	1	0
2	Paired stimulation	1	P_{glu}^*	$\eta (1-P_{glu})$
3	Paired stimulation + preNMDAR blockade	1	0	$+\eta$
4	Unpaired stimulation + photolysis	0	1	$-\eta$
5	Unpaired stimulation	0	P_{glu}^*	$-\eta (P_{glu})$
6	Unpaired stimulation + preNMDAR blockade	0	0	0

*Actual value will vary across synapses in this condition and is therefore represented as the variable P_{glu}.

For each category, we plotted initial P_r against final P_r for all synapses within the category, and superimposed the model's predictions as a red trend line (Figure 8D). The model's predictions were compared to a simple linear model, derived as a line of best fit (grey line; Figure 8D) for the data in the each category. The model consistently achieved a predictive power that was comparable to that of the line of best fit (Figure 8D,E), with the exception of category 4. Synapses in this condition received glutamate photolysis during unpaired stimulation and therefore underwent augmented depression. The model tended to overestimate the amount of depression for synapses with a low initial P_r and underestimate the amount of depression for synapses with a high initial P_r. However, the model's deviations from the line of best fit did not achieve statistical significance ($p=0.11$; Figure 8E), likely owing to a small number of data points ($n=13$) in this category. Across all 6 categories the model's explanatory power was not different from the lines of best fit ($p=0.44$; Figure 8E), despite only having a single free parameter (η, the learning rate) as compared with a total of 12 free parameters used by the lines of best fit (2 free parameters per line, the slope and the intercept). Consequently, the model achieved a

substantially better (i.e. lower) Bayesian Information Criterion (BIC) than the lines of best fit ($BIC_{lines\ of\ best\ fit} - BIC_{model} = 34.97$). This was also the case when we combined categories having similar trends (category 1 and 6) to minimize the free parameters used by the lines of best fit from 12 to 10 ($BIC_{lines\ of\ best\ fit} - BIC_{model} = 24.25$). Thus, a simple and parsimonious mathematical learning rule is capable of effectively predicting changes in P_r across a range of experimental conditions.

Discussion

We have explored the mechanisms of presynaptic plasticity at CA3-CA1 synapses in hippocampal slices. Based on our findings we present a unified framework of presynaptic plasticity, which suggests that, at active presynaptic terminals, changes in P_r are driven by two processes: 1) postsynaptic depolarization, which promotes increases in P_r through the L-VGCC-dependent release of NO from neuronal dendrites (LTP-promoting process), and 2) glutamate release, which promotes decreases in P_r through presynaptic NMDAR activation (LTD-promoting process). Both processes operate together to tune presynaptic function, with net changes in P_r depending on the strength of each process during presynaptic activity. (Figure 8A,B). Consequently, we found that pairing presynaptic activity with strong postsynaptic depolarization in glutamate receptor blockade produced the greatest increase in P_r, whereas pairing presynaptic activity with glutamate photolysis in the absence of postsynaptic depolarization produced the greatest decrease in P_r.

Presynaptic LTP can occur in the absence of synapse-specific glutamate signalling

Importantly, the mechanism of plasticity proposed in this study enables presynaptic terminals releasing little or no glutamate to become potentiated provided that their activity is accompanied by strong postsynaptic depolarization. This feature of presynaptic LTP may have important implications for plasticity. Most central synapses have low glutamate release probabilities, with some synapses appearing to release no glutamate in response to presynaptic stimulation [48, 49] This is true for synapses recorded in both *in*

vitro preparations from young rodents and *ex vivo* preparations from adult rodents. In fact, a recent electron microscopy study has identified that a significant portion of synapses (up to 35-50%) in the adult rodent hippocampus have presynaptic zones lacking synaptic vesicles in their near proximity (<170nm); these so-called "nascent zones" have been hypothesized to be functionally silent [50]. Although the existence of *bona fide* presynaptically silent synapses remains controversial [48], the low release probabilities of central synapses suggests that it is possible that activity at a presynaptic terminal may not elicit glutamate release at the synapse, but may still coincide with strong postsynaptic depolarization, driven by glutamate release at other co-active synapses. Under such conditions the presynaptic mechanisms of plasticity elucidated in this study, could enable the efficient induction of LTP at the presynaptic terminal, thereby allowing Hebb's postulate to be fulfilled, even under conditions of little or no glutamate release.

Our finding that presynaptic enhancements can occur without glutamatergic signalling at the synapse raises the question as to why many studies show that LTP induction can be abolished or impaired by blockade of one or more glutamate receptor subtypes [47, 51, 52]. Reconciliation of this discrepancy is readily achieved by recognizing that antagonists to AMPA, NMDA, and mGlu receptors can all reduce the level of postsynaptic spiking generated by synaptic stimulation, since all of these receptors have been shown to contribute to postsynaptic depolarization [33, 53-55]. Given that we find presynaptic changes rely on the voltage-dependent release of NO, it is possible that blockade of any of these glutamate receptor classes would abolish or reduce presynaptic LTP in an indirect way, by reducing postsynaptic depolarization and the activation of L-VGCCs. This may explain, in part, why experimental manipulations that augment the levels of postsynaptic depolarization reliably rescue LTP in AMPAR [47, 56], NMDAR [8, 11-13, 57-61] and mGluR blockade[62]. Importantly, our LTP induction protocol circumvented the need for any glutamate receptor-dependent depolarization during paired stimulation, as strong postsynaptic spiking was elicited by somatic current injection. Based on these results, we would argue that the physiological role of glutamate release in presynaptic potentiation is

for driving postsynaptic spiking as opposed to conveying a synapse-specific signal; this contrasts with the role of glutamate release in postsynaptic plasticity, in which synapse-specific activation of postsynaptic NMDARs is necessary for LTP induction.

While our approach for inducing LTP resembles that of traditional spike-timing dependent plasticity (STDP) protocols, which rely on NMDAR activation [63], there is a key difference. In our study, postsynaptic depolarization took the form of complex spikes, which included a brief period (7-10 ms) depolarization before the first spike. This period of subthreshold depolarization is known to facilitate the induction of LTP, possibly by inactivating voltage-gated potassium channels within the dendrite, which otherwise impede action potential backpropagation [64-68]. Moreover, these emulated potentials, like complex spikes recorded in vivo [32], contained broadened action potentials, which likely reflect strong depolarization in the dendrites [66, 68]. Consequently, the postsynaptic waveforms used in our study were likely to generate stronger levels of postsynaptic depolarization, and in a manner independent of glutamate release and NMDAR activation, than those used in STDP studies.

Presynaptic LTP requires L-VGCC and nitric oxide signalling

In our study, we demonstrate the importance of L-VGCC signalling in presynaptic potentiation, consistent with findings from other laboratories [10-13]. Since L-VGCCs have high voltage activation thresholds, presynaptic potentiation will require strong levels of postsynaptic depolarization, which may explain why presynaptic enhancements are not always reported in the literature[8]. It is very likely that the successful induction of presynaptic LTP depend on the levels of postsynaptic depolarization achieved during tetanus [10, 12], which in turn will be influenced by a variety of experimental factors, including the frequency and intensity of tetanic stimulation. L-VGCCs also exhibit voltage-dependent inactivation during extended periods of depolarization (>1s) [69, 70]. As such, the use of pairing protocols, in which the postsynaptic cell is voltage clamped at 0mV for prolonged periods of time (>10s) during presynaptic stimulation, are likely to be

unsuitable for driving presynaptic enhancements, despite being commonly used to drive postsynaptic enhancements [14].

It has long been recognized that the induction of LTP at the presynaptic locus requires a retrograde signal [71]. The most promising candidate is NO[9]. The role of NO in LTP has been a source of much controversy, and some studies have concluded that NO signalling is not necessary in LTP induction[9]. However, given that NO is likely to be important for presynaptic strengthening, the effect of NO signalling on synaptic plasticity will depend on whether presynaptic enhancements are obtained following LTP induction [14]. Indeed, studies that actually confirm presynaptic changes following LTP induction, including our own, consistently demonstrate that presynaptic enhancements depend on the synthesis and release of NO in both acute and cultured hippocampal preparations [72-75].

It has generally been assumed that NO synthesis is dependent on Ca^{2+} influx from postsynaptic NMDARs [9]; however, several studies have demonstrated that induction of presynaptic LTP is possible in NMDAR blockade suggests that this signalling pathway is not necessary for presynaptic potentiation [11-13]. Consistent with this notion, in our experiments, we found that specific blockade of postsynaptic NMDARs using intracellular application of MK-801 had no effect on changes in P_r induced by paired stimulation. Instead, we found an alternative pathway for NO synthesis that was crucial for presynaptic strengthening, and that depended on strong postsynaptic depolarization and activation of L-VGCCs. The differential importance of NO signalling mediated by NMDARs and L-VGCCs in presynaptic LTP may result from differences in the magnitude, kinetics, and/or spatial extent of NO signalling associated with the activation of each channel. Unfortunately, the poor sensitivity of NO-indicator dyes makes this possibility difficult to investigate with currently available tools.

Several groups have demonstrated that exogenous NO can potentiate synaptic transmission, and that this potentiation is restricted to synapses that are active during NO release [76, 77]. Here we extend these findings by showing that photolysis of NO at single

synapses can actually drive increases in Pr, and that this increase can occur in the absence of glutamatergic signalling. Moreover, we demonstrate that the potentiating effects of NO are not only restricted to active synapses, but specifically at synapses whose activity precede, rather than follow, NO release; thus, the requirements of NO signalling are consistent with those of Hebbian and spike-timing dependent plasticity[63]. It is important to mention that some groups have found no effect of exogenous NO application on synaptic plasticity [8, 9]. However, like glutamate, the effects of NO will depend on the spatiotemporal dynamics of NO signalling and the pattern of concurrent synaptic activity, which will likely vary across studies; therefore it is not surprising that NO application, like that of glutamate, can potentiate, depress, or have no effect on synaptic input depending on experimental conditions[14].

Glutamate drives presynaptic LTD via presynaptic NMDAR signalling

At active presynaptic terminals, whereas postsynaptic depolarization drives increases in P_r, we show, unexpectedly, that glutamate release drives decreases in P_r by acting on presynaptic NMDA receptors. We found that presynaptic NMDAR signalling operated both during LTP and LTD induction paradigms to reduce P_r. This finding suggests that the potentiating effects of postsynaptic depolarization and the depressing effects of endogenous glutamate release occur simultaneously during synaptic activity, regardless of the nature of postsynaptic depolarization. Thus, the processes underlying LTP and LTD induction are not temporally distinct mechanisms as traditionally believed, but operate jointly to tune synaptic function during presynaptic activity. Our results may explain why sometimes the same pairing protocol that produces LTP at low P_r synapses, produces LTD at high P_r synapses; presumably the postsynaptic depolarization achieved by such protocols is not of sufficient magnitude to prevent the depressing effects of glutamate release at high P_r synapses [22, 23]. At neocortical synapses, presynaptic NMDARs have been implicated in the induction of LTD; although their pharmacological inhibition does not appear to effect LTP [41, 78]. It is possible that the low frequency (0.2Hz) of

presynaptic stimulation used during LTP induction in these studies did not result in sufficient levels of glutamate release to elicit presynaptic depression via presynaptic NMDAR activation. By contrast, in our study LTP induction involved presynaptic stimulation at a theta frequency, which is effective at promoting glutamate release at the synapse [24]. As such, the inhibitory effects of presynaptic NMDARs on LTP may only be evident at higher stimulation frequencies.

Presynaptic NMDARs may, however, operate at lower stimulation frequencies in the context of spike-timing dependent plasticity. Recently, it was shown that low-frequency (0.2Hz), anti-causal pairing of pre- and post- synaptic spiking induced presynaptic LTD at hippocampal synapses, in a manner dependent on presynaptic NMDAR signalling [25]. This form of LTD, in addition to glutamate release, required endocannabinoid and astrocytic signalling, similar to spike-timing dependent LTD in the neocortex [42].

Previously we have demonstrated that presynaptic NMDARs at hippocampal synapses facilitate transmitter release during theta stimulation [24]. Given our current findings, presynaptic NMDARs appear to be important for presynaptic facilitation in the short-term, but presynaptic depression in the long-term. Presynaptic NMDAR in the neocortex also appear to facilitate both evoked and spontaneous glutamate release, and yet are similarly implicated in presynaptic LTD [44]. It may appear peculiar for a single protein to mediate seemingly disparate functions; however, another way to view the presynaptic NMDAR is as a dynamic regulator of presynaptic activity, appropriately tuning glutamate release depending on the patterns of pre- and postsynaptic activity. As such, the receptor may aid glutamate release during theta-related activity, but, triggers presynaptic LTD when this release fails to elicit sufficiently strong postsynaptic depolarization.

Presynaptic plasticity optimally tunes glutamate release

We found a simple mathematical framework [$\Delta P_r = \eta (P_{depol}-P_{glu})$] could predict changes in P_r based on a mismatch between 1) the probability that presynaptic activity is

accompanied by strong depolarization (P_{depol}) and 2) the probability that presynaptic activity is accompanied by glutamate release (P_{glu}) during synaptic stimulation. According to this model, presynaptic plasticity is driven only when there is a mismatch between P_{glu} and P_{depol}. Plasticity, by changing P_r, works to drive the value of P_{glu} closer to that of P_{depol}. This has a very intuitive interpretation. P_{glu} is a measure of the synapses ability to drive postsynaptic activity. P_{depol} is a measure of the synapse's ability to predict postsynaptic activity. By driving the value of P_{glu} closer to P_{depol}, presynaptic plasticity changes a synapse's ability to drive postsynaptic activity, so that it matches its ability to predict postsynaptic activity.

It is important to recognize that P_{glu} will not only depend on basal P_r, but also on the pattern of presynaptic activity, owing to the effects of short-term plasticity [79]. Moreover, for any given pattern of pre- and post- synaptic activity, there exists a value of P_r for which P_{glu} will equal P_{depol}. That is, there exists a value of P_r for which the probability of glutamate release for a given pattern of presynaptic stimulation (P_{glu}) will be equal to the probability that presynaptic stimulation is accompanied by strong postsynaptic depolarization (P_{depol}). The model predicts that this value of P_r represents a target value that all synapses will tend to for a given pattern of pre- and post- synaptic activity. Synapses below this target value will be potentiated because $P_{depol}>P_{glu}$, whereas those above this target value will be depressed because $P_{depol}<P_{glu}$. This can explain why in the literature, P_r has previously been reported to tend to a certain value when a particular pattern of pre- and post- synaptic stimulation is applied [22].

According to our model, the target P_r value given by pairing high frequency presynaptic stimulation with strong postsynaptic depolarization is lower than pairing low frequency presynaptic stimulation with strong postsynaptic depolarization. In both cases, P_{depol} is high, meaning that presynaptic plasticity will continue to drive P_r until P_{glu} is also high. However, with high frequency stimulation, a low target P_r achieves a high P_{glu}. In contrast, with lower frequency stimulation, a higher target P_r is required to achieve a similarly high

P_{glu}. Consequently, as we showed in our experiments with Figure 1, when paired with strong postsynaptic depolarization, low frequency presynaptic stimulation will produce greater presynaptic potentiation than higher frequency stimulation. That P_r is kept low at synapses where presynaptic bursts are good predictors of postsynaptic spiking ensures that only presynaptic bursts mobilize glutamate, rather than individual presynaptic stimuli, which may not be good predictors of postsynaptic spiking. Therefore, presynaptic plasticity appears to tune P_r, such that the patterns of presynaptic activity that predict postsynaptic spiking are the ones that most efficiently drive glutamate release.

Methods

Cultured hippocampal slices

Cultured hippocampal slices (350µm) were prepared from male Wistar rats (P7-P8), as previously described[27]. Slices were maintained in media at 37°C and 5% CO_2 for 7-14 days prior to use. Media comprised of 50% Minimum Essential Media, 25% heat-inactivated horse serum, 23% Earl's Balanced Salt Solution, and 2% B-27 with added glucose (6.5g/L), and was replaced every 2-3 days. During experimentation, slices were perfused with artificial cerebrospinal fluid (ACSF; 1mL/min), which was constantly bubbled with carbogen (95% O_2 and 5% CO_2) and heated to achieve near-physiological temperatures in the bath (31-33°C). ACSF contained (in mM) 145 NaCl, 16 $NaHCO_3$, 11 glucose, 2.5 KCl, 2-3 $CaCl_2$, 1-2 $MgCl_2$, 1.2 NaH_2PO_4, and, to minimize photodynamic damage, 0.2 ascorbic acid and 1 Trolox.

Acute hippocampal slices

Coronal acute hippocampal slices (400µm) were prepared from 2-4 week old male Wistar rats. Tissue was dissected in a sucrose-based ACSF solution (in mM: 85 NaCl, 65 sucrose, 26 $NaHCO_3$, 10 glucose, 7 $MgCl_2$, 2.5 KCl, 1.2 NaH_2PO_4, and 0.5 $CaCl_2$). The whole brain was sliced into coronal sections using a Microm HM 650V vibratome (Thermo Scientific) and hippocampi were carefully dissected from each slice. Hippocampal tissue were allowed to recover at room temperature in normal ACSF (120 NaCl, 2.5 KCl, 2 $CaCl_2$, 1 $MgCl_2$, 1.2 NaH_2PO_4, 26 $NaHCO_3$, and 11 glucose), which was bubbled with 95% O_2 and 5% CO_2. Slices were given at least 1 hour to recover before use. During experimentation, slices were perfused with ACSF (3mL/min) containing picrotoxin (100µM). The ACSF was constantly bubbled with carbogen (95% O_2 and 5% CO_2) and heated to achieve near-physiological temperatures in the bath (31-33°C).

Patch recordings

To minimize the effects of dialysis in electrophysiological experiments, CA1 pyramidal neurons were recorded from either using high resistance patch electrodes (18-25MΩ) filled with standard internal solution (in mM: 135 KGluconate, 10 KCl, 10 HEPES, 2 $MgCl_2$, 2 Na_2ATP and 0.4 Na_3GTP) or low resistance (4-8MΩ) patch electrodes filled with ATP regenerating solution (in mM: 130 KGluconate, 10 KCl, 10 HEPES, 10 NaPhosphocreatine, 4 MgATP, 0.4 Na_3GTP and 50U/mL creatine phosphokinase) [57]. The recording method used in a given experiment is clearly indicated in the text. In imaging experiments, unless otherwise stated, low-resistance patch electrodes (4-8MΩ) containing standard internal solution were used to transiently load cells with dye. Cells were then subsequently re-patched for the purposes of LTP induction.

Stimulation protocols

A glass electrode (4-8MΩ), filled with ACSF, was placed in stratum radiatum, within 200µm of the recorded cell. In experiments with glutamate receptor blockade, two stimulation electrodes were placed within 50-70µm of the recorded cell. Continuous basal stimulation (0.05-0.10Hz) was present for all experiments, and was only interrupted to deliver paired-pulse or tetanic stimulation. Stimulation intensity was adjusted to evoke a 5-10mV EPSP; pulse duration was set at 100µs. Paired-pulse stimulation consisted of 2 presynaptic stimuli delivered 70ms apart. LTP induction consisted of 60 pulses delivered at 5Hz. For LTP induction, postsynaptic depolarization took the form of a complex spike. To emulate a complex spike, we injected a postsynaptic current waveform (2-3nA) that was approximately 60ms in duration (7-10ms rising phase, 20ms plateau phase, 30-33ms falling phase) and resulted in 3-6 spikes at ~100Hz. Stimulating electrodes were placed within 50-70µm of the soma to ensure that postsynaptic depolarization reached stimulated synapses without significant attenuation. LTD induction consisted of presynaptic stimulation (60-120 pulses at 5Hz), delivered in the absence of postsynaptic depolarization. In some cases, stimulation was delivered while the postsynaptic neuron was hyperpolarized to prevent spiking. In other cases, stimulation proceeded without any

postsynaptic current injection; in these instances the neuron rarely generated postsynaptic spikes.

Electrophysiology and analysis

All electrophysiological data was recorded using WinWCP (Strathclyde Electrophysiology Software) and analyzed using Clampfit (Axon Insturments) and Excel (Microsoft). The initial EPSP slope, calculated during the first 3ms of the response, was used to analyze changes in the EPSP throughout the recording. All data was normalized to the average EPSP slope recorded during baseline to yield ΔEPSP slope. Paired pulse ratio (PPR) was calculated as the average EPSP slope evoked by the second stimulation pulse divided by the average EPSP slope evoked by the first stimulation pulse, as previously described [80]; averages were calculated from 10-20 paired pulse trials. Decreases in PPR are thought to reflect increases in release probability [81]. The coefficient of variation parameter CV^{-2}, which reflects the $mean^2$/variance, was calculated using the EPSP slopes collected over 25-30 trials. The CV^{-2} calculated from 25-30 stimulation trials taken 30 minutes following LTP induction was normalized to the CV^{-2} calculated from 25-30 stimulation trials at baseline to yield ΔCV^{-2}. For each experiment, ΔCV^{-2} was plotted against mean ΔEPSP slope. When ΔCV^{-2} > mean ΔEPSP slope, activity-induced enhancements in EPSP slope are thought to predominantly reflect increases in release probability *[82]*. To control for the effects of incomplete drug washout, for experiments with glutamate receptor blockade, ΔEPSP slope and ΔCV^{-2} for the tetanized pathway were normalized to values obtained for the control pathway.

Ca^{2+} imaging and analysis

In experiments only requiring Ca^{2+} imaging without electrophysiological recordings, CA1 pyramidal neurons were loaded with Ca^{2+} sensitive dye using a low resistance patch electrode (4-8 MΩ) containing 1mM Oregon Green Bapta-1 (Invitrogen) dissolved in standard internal solution. The cell was loaded for 45-60s, after which the patch electrode

was slowly withdrawn over the course of 1-2 minutes using a piezoelectric drive. Withdrawal of the electrode was very rarely associated with a rise in intracellular Ca^{2+}, suggesting that the procedure caused minimal damage to the cell.

A stimulating glass electrode (4-8MΩ) was then brought near (5-20µm) to a branch of imaged dendrite within stratum radiatum. For visualization purposes, electrode tips were coated with bovine serum albumin Alexa 488 conjugate (Invitrogen), as previously described [83]. Briefly, a 0.05% BSA-Alexa 488 solution was made with 0.1M phosphate-buffered saline containing 3mM NaN_3. Pipette tips were placed in the solution for 2-5 minutes.

Ca^{2+} transients were evoked with pairs of stimuli (70ms apart) and monitored by restricting confocal laser scanning to a single line through the spine and underlying dendrite; images were acquired at a rate of 500Hz and analyzed using ImageJ and Microsoft excel. Increases in fluorescence intensity ($\Delta F/F = F_{transient} - F_{baseline}/F_{baseline}$) following the delivery of the first stimulus reflect successful glutamate release from the presynaptic terminal [27, 37]. The proportion of successful fluorescent responses to the first stimulus across stimulation trials was used to calculate P_r. P_r was assessed on the basis of 15-40 trials at baseline and at 25-30 minutes post-tetanus. For high P_r synapses (>0.8) the number of stimulation trials was limited to 15-20 to avoid photodynamic damage that results from imaging the frequent Ca^{2+} responses generated at these synapses. For all other synapses, P_r was generally assessed using 30 trials of stimulation. Synapses with initial P_r values of 0-0.7 were used for LTP experiments. Since our LTD protocol did not elicit depression in low P_r synapses (Figure 2), for the majority of LTD experiments, synapses with P_r values of 0.5-1.0 were used. In experiments involving glutamate receptor blockade, P_r was measured prior to drug application at baseline, and measured post-tetanus, following drug washout. In experiments involving NMDAR blockade, using either AP5 or MK-801, drugs were present for the duration of the

experiment and, therefore, present for both the baseline and post-tetanus measurements of Pr.

Photolysis

A 405nm laser (Photonics) was used for photolysis. The laser was focussed to a small spot (~1.2µm diameter) by overfilling the back aperture of a 60x water-immersion lens (Olympus). Electrode manipulators and recording chambers were mounted on a movable stage, which enabled a region above the spine head to be positioned beneath the photolysis spot. Laser exposure was controlled using a fast shutter (LS6; Uniblitz). For glutamate photolysis, MNI glutamate (Tocris) was focally delivered through a glass pipette (4-8MΩ; 10mM MNI glutamate) using a picosprtizer (Science Products). Laser exposure was limited to ~2ms and, in each experiment, the laser intensity (0.5-2mW) was adjusted to generate a Ca^{2+} response in the underlying spine that was comparable to the response generated by electrical stimulation. For NO photolysis, 0.5-1mM $RuNOCl_3$ (Sigma) was bath applied and uncaged using 30-60 laser pulses (25ms; 2mW) delivered at 5Hz; presynaptic stimulation either preceded or followed NO photolysis by 10ms. Using the NO-indicator, DAF-FM (Invitrogen), we estimated that a given laser pulse liberated approximately 4-7nM of NO.

Nitric oxide imaging

Experiments were carried out in Tyrodes buffer (in mM: 120 NaCl, 2.5 KCl, 30 glucose, 4 $CaCl_2$, 0 $MgCl_2$, and 25 HEPES) containing 50µM AP5, 10µM NBQX, 500µM MCPG, and 100µM LY341495 (Abcam) to block glutamate receptors, as well as 1µM Bay K-8644 (Abcam) to prevent L-type voltage gated calcium channel desensitization during K+ application. CA1 pyramidal neurons were transiently patched with glass electrodes (4-8MΩ) containing standard internal solution with 250µM of DAF-FM (Invitrogen) and loaded for 60s before withdrawing the electrode. Apical dendrites, often secondary or tertiary branches, within 100µm of the soma were imaged at one focal plane, once prior

to, and once 5-10s following, the addition of a high K^+ Tyrodes solution (in mM: 32.5 NaCl, 90 KCl, 30 glucose, 4 $CaCl_2$, 0 $MgCl_2$, 25 HEPES, 50µM AP5, 10µM NBQX, 500µM MCPG, and 100µM LY341495). Laser power and exposure was kept to a minimum to avoid photobleaching. DAF-FM basal fluorescence was not quenched by intracellular addition of cPTIO.

Pharmacology

Glutamate receptor blockade was achieved using AP5 (50-100µM; Abcam), NBQX (10µM; Abcam), MCPG (500µM; Abcam) and LY341495 (100µM; Abcam). In experiments requiring both pre- and post- synaptic NMDARs to be blocked, either AP5 (50-100µM) or MK-801 (20µM) was added in bath for the duration of the experiment. In the case of MK-801, slices were pre-incubated with the drug for at least 1 hour prior to experimentation. Postsynaptic NMDA receptors were blocked by including MK-801 (0.5-2mM loaded for 60s via a 4-8MΩ patch electrode; Abcam) in the patch solution during Ca^{2+} dye loading. L-type voltage gated calcium channels were blocked with nitrendipine (20µM; Abcam). NO synthase was inhibited by incubation with L-NAME (100µM; Sigma), which started 20 minutes prior to experimentation. Extracellular NO was scavenged by bath application of cPTIO (50-100µM; Sigma). Intracellular NO was scavenged by including cPTIO (5mM; loaded for 60s via a 4-8MΩ patch electrode) in the patch solution during Ca^{2+} dye loading. Intracellular Ca^{2+} was chelated using a patch electrode containing 15mM K_4BAPTA in the place of 60mM KGluconate.

Mathematical model

The model $\Delta P_r = \eta(P_{depol}-P_{glu})$ was used to predict changes in P_r in our data set of imaged synapses, across all experimental conditions. Data was divided into 6 categories, depending on whether the effects of postsynaptic depolarization were present or absent, whether the effects of glutamate photolysis was present or absent, and whether the effects of presynaptic NMDAR signalling was present or absent. These 6 categories, along

with the models predictions for ΔP_r are shown in Figure 8C and are summarized in the table below.

No.	Effects present	P_{depol}	P_{glu}	$\Delta P_r = \eta (P_{depol}-P_{glu})$
1	Paired stimulation + photolysis	1	1	0
2	Paired stimulation	1	P_{glu}^*	$\eta (1-P_{glu})$
3	Paired stimulation + preNMDAR blockade	1	0	$+\eta$
4	Unpaired stimulation + photolysis	0	1	$-\eta$
5	Unpaired stimulation	0	P_{glu}^*	$-\eta (P_{glu})$
6	Unpaired stimulation + preNMDAR blockade	0	0	0

*Actual value will vary across synapses in this condition and is therefore represented as a variable.

The experimental data in each category are as follows.

Category 1 – included data from experiments in which the effects of postsynaptic depolarization and glutamate photolysis were present during presynaptic stimulation (Figure 2D, 7A). This included experiments in which MK-801 was applied intracellularly during photolysis (Figure 7A). For this category, P_{depol} was set to 1 and P_{glu} was set to 1.

Category 2 – included data from experiments in which the effects of postsynaptic depolarization and endogenous glutamate release were present during presynaptic stimulation (Figure 2D, 4B, 6B). This included experiments in which MK-801 was applied intracellularly (Figure 6B). For this category, P_{depol} was set to 1 and P_{glu} was calculated for each synapse based on: $P_{glu} = 0.475*\text{initial } P_r + 0.2175$, which was experimentally derived from data in Supplemental Figure 4.

Category 3 – included data from experiments in which the effects of postsynaptic depolarization were present but the effects of glutamate release were absent during presynaptic stimulation (Figure 6B,7A). This included experiments in which paired stimulation was delivered in full glutamate receptor or during bath application of AP5 or

MK-801 (Figure 6B). These also included pairing experiments involving glutamate photolysis, but in the presence of MK-801 in the bath (Figure 7A). For this category, P_{depol} was set to 1 and P_{glu} was set to 0.

Category 4 – included data from experiments in which the effects of postsynaptic depolarization were absent but the effects of glutamate photolysis was present during presynaptic stimulation (Figure 2E, 7C). This included experiments in which MK-801 was applied intracellularly during photolysis (Figure 7C). For this category, P_{depol} was set to 0 and P_{glu} was set to 1.

Category 5 – included data from experiments in which the effects of postsynaptic depolarization were absent but the effects of endogenous glutamate release were present during presynaptic stimulation (Figure 2E, 6D). This included experiments in which MK-801 was applied intracellularly during stimulation (Figure 6D). For this category, P_{depol} was set to 0 and P_{glu} was calculated for each synapse based on: $P_{glu} = 0.475*\text{initial } P_r + 0.2175$, which was experimentally derived from data in Supplemental Figure 4.

Category 6 – included data from experiments in which the effects of postsynaptic depolarization and glutamate release were both absent during presynaptic stimulation (Figure 4B, 5A, 6D, 7C). This included: 1) Experiments in which presynaptic stimulation was delivered in full glutamate receptor blockade, and unaccompanied by postsynaptic depolarization (Figure 4B). 2) Experiments conducted in full glutamate receptor blockade in which presynaptic stimulation was not delivered during postsynaptic depolarization (Figure 4B). 3) Experiments that took place in full glutamate receptor blockade and in which the effects of postsynaptic depolarization were abolished, either by nitrendipine, extracellular cPTIO, or intracellular cPTIO (Figure 5A). 4) Experiments conducted with AP5 or MK-801 present in the bath, and in which postsynaptic depolarization was absent (Figure 6D). 5) Experiments done with bath application of MK-801, and in which postsynaptic depolarization was absent but glutamate photolysis was present. (Figure 7C). For this category, P_{depol} was set to 0 and P_{glu} was set to 0.

The learning rate η was determined to be 0.35, this gave the best fit of the model on a small training set of 10 synapses, 5 of which that underwent paired stimulation and 5 of which that underwent unpaired stimulation.

For each category, the initial P_r was plotted against final P_r for all synapses within the category. The model's predictions were compared to that of a line of best fit, derived from simple linear regression. The model's predictions for final P_r were set to 1 if they were >1, and were set to 0 if they were <0. Differences in the variance explained by both the model and line of best fit was assessed for significance using an F-test. Bayesian Information Criterion (BIC) was calculated for the model and the lines of best fit as BIC = n*ln(RSS/n) + k*ln(n). Here, n is the number of data points (n=216), ln is the natural logarithm, RSS is the residual sum of squares and calculated by Σ(model predictions – actual value)^2, and k is the number of free parameters, which was 1 for the proposed model, and 12 for the lines of best fit (2 free parameters per line of best fit, the slope and the intercept). The BIC aids model selection by favouring models that have a high predictive power (explained variance) but a small number of free parameters. A difference of BIC > 10 between two models strongly favors the model with the smaller BIC value .

Statistical analysis

The statistical significance of comparisons was mainly assessed using two tailed, Mann-Whitney or Wilcoxon matched pairs tests, depending on whether the data was unpaired or paired, respectively. One sample t-tests were used to determine if average data significantly differed from an expected value. Pearson correlation coefficients were calculated to determine the significance of linear trends. Significance between trend lines was determined by using a Wilcoxon matched-pairs tests to examine the statistical difference between the two sets of residuals that resulted from fitting a given data set with two trend lines of interest. Averages and standard error of the mean (S.E.M.) are represented in the text as average±S.E.M.

References

1. Padamsey, Z. and N.J. Emptage, *Imaging synaptic plasticity.* Mol Brain, 2011. **4**: p. 36.
2. Bliss, T.V. and G.L. Collingridge, *Expression of NMDA receptor-dependent LTP in the hippocampus: bridging the divide.* Mol Brain, 2013. **6**: p. 5.
3. Larkman, A.U. and J.J. Jack, *Synaptic plasticity: hippocampal LTP.* Curr Opin Neurobiol, 1995. **5**(3): p. 324-34.
4. Lisman, J., *Long-term potentiation: outstanding questions and attempted synthesis.* Philos Trans R Soc Lond B Biol Sci, 2003. **358**(1432): p. 829-42.
5. Lisman, J. and S. Raghavachari, *A unified model of the presynaptic and postsynaptic changes during LTP at CA1 synapses.* Sci STKE, 2006. **2006**(356): p. re11.
6. Padamsey, Z. and N. Emptage, *Two sides to long-term potentiation: a view towards reconciliation.* Philos Trans R Soc Lond B Biol Sci, 2014. **369**(1633): p. 20130154.
7. Luscher, C. and R.C. Malenka, *NMDA receptor-dependent long-term potentiation and long-term depression (LTP/LTD).* Cold Spring Harb Perspect Biol, 2012. **4**(6).
8. Padamsey, Z. and N. Emptage, *Two sides to long-term potentiation: a view towards reconciliation.* Philos Trans R Soc Lond B Biol Sci, 2013. **369**(1633): p. 20130154.
9. Garthwaite, J. and C.L. Boulton, *Nitric oxide signaling in the central nervous system.* Annu Rev Physiol, 1995. **57**: p. 683-706.
10. Blundon, J.A. and S.S. Zakharenko, *Dissecting the components of long-term potentiation.* Neuroscientist, 2008. **14**(6): p. 598-608.
11. Zakharenko, S.S., et al., *Presynaptic BDNF required for a presynaptic but not postsynaptic component of LTP at hippocampal CA1-CA3 synapses.* Neuron, 2003. **39**(6): p. 975-90.
12. Bayazitov, I.T., et al., *Slow presynaptic and fast postsynaptic components of compound long-term potentiation.* J Neurosci, 2007. **27**(43): p. 11510-21.
13. Zakharenko, S.S., L. Zablow, and S.A. Siegelbaum, *Visualization of changes in presynaptic function during long-term synaptic plasticity.* Nat Neurosci, 2001. **4**(7): p. 711-7.
14. Padamsey, Z. and N.J. Emptage, *Two sides to LTP: a view towards reconciliation.* Philos Trans R Soc Lond B Biol Sci, 2013. ***In press.***
15. Pigott, B.M. and J. Garthwaite, *Nitric Oxide Is Required for L-Type Ca(2+) Channel-Dependent Long-Term Potentiation in the Hippocampus.* Front Synaptic Neurosci, 2016. **8**: p. 17.
16. Harvey, C.D. and K. Svoboda, *Locally dynamic synaptic learning rules in pyramidal neuron dendrites.* Nature, 2007. **450**(7173): p. 1195-200.
17. Matsuzaki, M., et al., *Structural basis of long-term potentiation in single dendritic spines.* Nature, 2004. **429**(6993): p. 761-6.
18. Makino, H. and R. Malinow, *AMPA receptor incorporation into synapses during LTP: the role of lateral movement and exocytosis.* Neuron, 2009. **64**(3): p. 381-90.
19. Ryan, T.A., N.E. Ziv, and S.J. Smith, *Potentiation of evoked vesicle turnover at individually resolved synaptic boutons.* Neuron, 1996. **17**(1): p. 125-34.
20. Slutsky, I., et al., *Enhancement of synaptic plasticity through chronically reduced Ca2+ flux during uncorrelated activity.* Neuron, 2004. **44**(5): p. 835-49.
21. Larkman, A., et al., *Presynaptic release probability influences the locus of long-term potentiation.* Nature, 1992. **360**(6399): p. 70-3.

22. Hardingham, N.R., et al., *Presynaptic efficacy directs normalization of synaptic strength in layer 2/3 rat neocortex after paired activity.* J Neurophysiol, 2007. **97**(4): p. 2965-75.
23. Saez, I. and M.J. Friedlander, *Plasticity between neuronal pairs in layer 4 of visual cortex varies with synapse state.* J Neurosci, 2009. **29**(48): p. 15286-98.
24. McGuinness, L., et al., *Presynaptic NMDARs in the Hippocampus Facilitate Transmitter Release at Theta Frequency.* Neuron, 2010. **68**(6): p. 1109-27.
25. Andrade-Talavera, Y., et al., *Presynaptic Spike Timing-Dependent Long-Term Depression in the Mouse Hippocampus.* Cereb Cortex, 2016. **26**(8): p. 3637-54.
26. Enoki, R., et al., *Expression of long-term plasticity at individual synapses in hippocampus is graded, bidirectional, and mainly presynaptic: optical quantal analysis.* Neuron, 2009. **62**(2): p. 242-53.
27. Emptage, N.J., et al., *Optical quantal analysis reveals a presynaptic component of LTP at hippocampal Schaffer-associational synapses.* Neuron, 2003. **38**(5): p. 797-804.
28. Thomas, M.J., et al., *Postsynaptic complex spike bursting enables the induction of LTP by theta frequency synaptic stimulation.* J Neurosci, 1998. **18**(18): p. 7118-26.
29. Remy, S. and N. Spruston, *Dendritic spikes induce single-burst long-term potentiation.* Proc Natl Acad Sci U S A, 2007. **104**(43): p. 17192-7.
30. Golding, N.L., N.P. Staff, and N. Spruston, *Dendritic spikes as a mechanism for cooperative long-term potentiation.* Nature, 2002. **418**(6895): p. 326-31.
31. Hardie, J. and N. Spruston, *Synaptic depolarization is more effective than back-propagating action potentials during induction of associative long-term potentiation in hippocampal pyramidal neurons.* J Neurosci, 2009. **29**(10): p. 3233-41.
32. Ranck, J.B., Jr., *Studies on single neurons in dorsal hippocampal formation and septum in unrestrained rats. I. Behavioral correlates and firing repertoires.* Exp Neurol, 1973. **41**(2): p. 461-531.
33. Grienberger, C., X. Chen, and A. Konnerth, *NMDA receptor-dependent multidendrite Ca(2+) spikes required for hippocampal burst firing in vivo.* Neuron, 2014. **81**(6): p. 1274-81.
34. Kowalski, J., et al., *Intrinsic membrane properties determine hippocampal differential firing pattern in vivo in anesthetized rats.* Hippocampus, 2016. **26**(5): p. 668-82.
35. Ward, B., et al., *State-dependent mechanisms of LTP expression revealed by optical quantal analysis.* Neuron, 2006. **52**(4): p. 649-61.
36. Grunditz, A., et al., *Spine neck plasticity controls postsynaptic calcium signals through electrical compartmentalization.* J Neurosci, 2008. **28**(50): p. 13457-66.
37. Emptage, N., T.V. Bliss, and A. Fine, *Single synaptic events evoke NMDA receptor-mediated release of calcium from internal stores in hippocampal dendritic spines.* Neuron, 1999. **22**(1): p. 115-24.
38. Sattler, R., et al., *Specific coupling of NMDA receptor activation to nitric oxide neurotoxicity by PSD-95 protein.* Science, 1999. **284**(5421): p. 1845-8.
39. Stanika, R.I., et al., *Comparative impact of voltage-gated calcium channels and NMDA receptors on mitochondria-mediated neuronal injury.* J Neurosci, 2012. **32**(19): p. 6642-50.
40. Rodriguez-Moreno, A., et al., *Presynaptic Self-Depression at Developing Neocortical Synapses.* Neuron, 2012. **77**: p. 35-42.
41. Rodriguez-Moreno, A. and O. Paulsen, *Spike timing-dependent long-term depression requires presynaptic NMDA receptors.* Nat Neurosci, 2008. **11**(7): p. 744-5.
42. Min, R. and T. Nevian, *Astrocyte signaling controls spike timing-dependent depression at neocortical synapses.* Nat Neurosci, 2012. **15**(5): p. 746-53.

43. Nevian, T. and B. Sakmann, *Spine Ca2+ signaling in spike-timing-dependent plasticity.* J Neurosci, 2006. **26**(43): p. 11001-13.
44. Corlew, R., et al., *Presynaptic NMDA receptors: newly appreciated roles in cortical synaptic function and plasticity.* Neuroscientist, 2008. **14**(6): p. 609-25.
45. Corlew, R., et al., *Developmental switch in the contribution of presynaptic and postsynaptic NMDA receptors to long-term depression.* J Neurosci, 2007. **27**(37): p. 9835-45.
46. Cormier, R.J. and P.T. Kelly, *Glutamate-induced long-term potentiation enhances spontaneous EPSC amplitude but not frequency.* J Neurophysiol, 1996. **75**(5): p. 1909-18.
47. Holbro, N., et al., *AMPA receptors gate spine Ca(2+) transients and spike-timing-dependent potentiation.* Proc Natl Acad Sci U S A, 2010. **107**(36): p. 15975-80.
48. Voronin, L.L. and E. Cherubini, *'Deaf, mute and whispering' silent synapses: their role in synaptic plasticity.* J Physiol, 2004. **557**(Pt 1): p. 3-12.
49. Stevens, C.F., *Neurotransmitter release at central synapses.* Neuron, 2003. **40**(2): p. 381-8.
50. Bell, M.E., et al., *Dynamics of Nascent and Active Zone Ultrastructure as Synapses Enlarge During Ltp in Mature Hippocampus.* J Comp Neurol, 2014. **522**(17): p. 3861-84.
51. Collingridge, G.L., S.J. Kehl, and H. McLennan, *Excitatory amino acids in synaptic transmission in the Schaffer collateral-commissural pathway of the rat hippocampus.* J Physiol, 1983. **334**: p. 33-46.
52. Bashir, Z.I., et al., *Induction of LTP in the hippocampus needs synaptic activation of glutamate metabotropic receptors.* Nature, 1993. **363**(6427): p. 347-50.
53. Schiller, J. and Y. Schiller, *NMDA receptor-mediated dendritic spikes and coincident signal amplification.* Curr Opin Neurobiol, 2001. **11**(3): p. 343-8.
54. Grover, L.M. and C. Yan, *Blockade of GABAA receptors facilitates induction of NMDA receptor-independent long-term potentiation.* J Neurophysiol, 1999. **81**(6): p. 2814-22.
55. Chemin, J., et al., *Mechanisms underlying excitatory effects of group I metabotropic glutamate receptors via inhibition of 2P domain K+ channels.* EMBO J, 2003. **22**(20): p. 5403-11.
56. Fuenzalida, M., et al., *Role of AMPA and NMDA receptors and back-propagating action potentials in spike timing-dependent plasticity.* J Neurophysiol, 2010. **103**(1): p. 47-54.
57. Kullmann, D.M., et al., *Ca2+ entry via postsynaptic voltage-sensitive Ca2+ channels can transiently potentiate excitatory synaptic transmission in the hippocampus.* Neuron, 1992. **9**(6): p. 1175-83.
58. Huber, K.M., M.D. Mauk, and P.T. Kelly, *Distinct LTP induction mechanisms: contribution of NMDA receptors and voltage-dependent calcium channels.* J Neurophysiol, 1995. **73**(1): p. 270-9.
59. Grover, L.M. and T.J. Teyler, *N-methyl-D-aspartate receptor-independent long-term potentiation in area CA1 of rat hippocampus: input-specific induction and preclusion in a non-tetanized pathway.* Neuroscience, 1992. **49**(1): p. 7-11.
60. Grover, L.M., et al., *LTP in hippocampal area CA1 is induced by burst stimulation over a broad frequency range centered around delta.* Learn Mem, 2009. **16**(1): p. 69-81.
61. Morgan, S.L. and T.J. Teyler, *Electrical stimuli patterned after the theta-rhythm induce multiple forms of LTP.* J Neurophysiol, 2001. **86**(3): p. 1289-96.
62. Wilsch, V.W., et al., *When are class I metabotropic glutamate receptors necessary for long-term potentiation?* J Neurosci, 1998. **18**(16): p. 6071-80.
63. Dan, Y. and M.M. Poo, *Spike timing-dependent plasticity of neural circuits.* Neuron, 2004. **44**(1): p. 23-30.

64. Watanabe, S., et al., *Dendritic K+ channels contribute to spike-timing dependent long-term potentiation in hippocampal pyramidal neurons.* Proc Natl Acad Sci U S A, 2002. **99**(12): p. 8366-71.
65. Gasparini, S., et al., *Associative pairing enhances action potential back-propagation in radial oblique branches of CA1 pyramidal neurons.* J Physiol, 2007. **580**(Pt.3): p. 787-800.
66. Hoffman, D.A., et al., *K+ channel regulation of signal propagation in dendrites of hippocampal pyramidal neurons.* Nature, 1997. **387**(6636): p. 869-75.
67. Johnston, D., et al., *Regulation of back-propagating action potentials in hippocampal neurons.* Curr Opin Neurobiol, 1999. **9**(3): p. 288-92.
68. Migliore, M., et al., *Role of an A-type K+ conductance in the back-propagation of action potentials in the dendrites of hippocampal pyramidal neurons.* J Comput Neurosci, 1999. **7**(1): p. 5-15.
69. Hofmann, F., L. Lacinova, and N. Klugbauer, *Voltage-dependent calcium channels: from structure to function.* Rev Physiol Biochem Pharmacol, 1999. **139**: p. 33-87.
70. Lacinova, L. and F. Hofmann, *Ca2+- and voltage-dependent inactivation of the expressed L-type Ca(v)1.2 calcium channel.* Arch Biochem Biophys, 2005. **437**(1): p. 42-50.
71. Williams, J.H., et al., *Arachidonic acid induces a long-term activity-dependent enhancement of synaptic transmission in the hippocampus.* Nature, 1989. **341**(6244): p. 739-42.
72. Nikonenko, I., P. Jourdain, and D. Muller, *Presynaptic remodeling contributes to activity-dependent synaptogenesis.* J Neurosci, 2003. **23**(24): p. 8498-505.
73. Stanton, P.K., et al., *Imaging LTP of presynaptic release of FM1-43 from the rapidly recycling vesicle pool of Schaffer collateral-CA1 synapses in rat hippocampal slices.* Eur J Neurosci, 2005. **22**(10): p. 2451-61.
74. Johnstone, V.P. and C.R. Raymond, *A protein synthesis and nitric oxide-dependent presynaptic enhancement in persistent forms of long-term potentiation.* Learn Mem, 2011. **18**(10): p. 625-33.
75. Ratnayaka, A., et al., *Recruitment of resting vesicles into recycling pools supports NMDA receptor-dependent synaptic potentiation in cultured hippocampal neurons.* J Physiol, 2012. **590**(Pt 7): p. 1585-97.
76. Arancio, O., et al., *Nitric oxide acts directly in the presynaptic neuron to produce long-term potentiation in cultured hippocampal neurons.* Cell, 1996. **87**(6): p. 1025-35.
77. Zhuo, M., et al., *Nitric oxide and carbon monoxide produce activity-dependent long-term synaptic enhancement in hippocampus.* Science, 1993. **260**(5116): p. 1946-50.
78. Rodriguez-Moreno, A., et al., *Presynaptic self-depression at developing neocortical synapses.* Neuron, 2013. **77**(1): p. 35-42.
79. Dobrunz, L.E. and C.F. Stevens, *Heterogeneity of release probability, facilitation, and depletion at central synapses.* Neuron, 1997. **18**(6): p. 995-1008.
80. Kim, J. and B.E. Alger, *Random response fluctuations lead to spurious paired-pulse facilitation.* J Neurosci, 2001. **21**(24): p. 9608-18.
81. Schulz, P.E., E.P. Cook, and D. Johnston, *Changes in paired-pulse facilitation suggest presynaptic involvement in long-term potentiation.* J Neurosci, 1994. **14**(9): p. 5325-37.
82. Faber, D.S. and H. Korn, *Applicability of the coefficient of variation method for analyzing synaptic plasticity.* Biophys J, 1991. **60**(5): p. 1288-94.
83. Ishikawa, D., et al., *Fluorescent pipettes for optically targeted patch-clamp recordings.* Neural Netw, 2010. **23**(6): p. 669-72.

Acknowledgements

Z.P was funded by a Clarendon Scholarship, a scholarship from the National Science and Engineering Research Council of Canada, and a Junior Research Fellowship from Magdalen College, University of Oxford. Experimental work was funded by the Medical Research Council. The funders had no role in study design, data collection and analysis, decision to publish, or preparation of the manuscript

Author Contributions

Z.P. conceived the idea for study. Z.P. and N.J.E. designed the experiments. Z.P. and R.T. conducted the experiments and analyzed the data. Z.P. and N.J.E prepared the manuscript. All authors have seen and approved the manuscript.

Competing Interests

The authors declare that they have no competing interests.

Figure legends

Figure 1. High frequency presynaptic activity inhibits presynaptic LTP and augments presynaptic LTD. (A,D) Average $EPSP_{slope}$ recordings obtained from whole-cell patch clamp of CA1 neurons. Following baseline recording, 60 presynaptic stimuli were delivered at 5Hz, and were either delivered in the presence (paired stimulation) or absence (unpaired stimulation) of strong postsynaptic depolarization. Presynaptic stimuli were either delivered as single pulses, or high frequency presynaptic bursts consisting of two pulses delivered 5ms apart. High frequency bursts generated significantly less LTP with paired stimulation, and more LTD with unpaired stimulation, than did single pulse stimulation. Sample EPSP traces at baseline (black trace) and 30 minutes after the pairing protocol (red trace) are shown as an inset above. Average changes in **(B,E)** $EPSP_{slope}$ and **(C,F)** paired pulse ratio (PPR), averaged between 25-30 minutes post-pairing are shown. Error bars represent S.E.M. (n=5-8 slices per condition). Asterisks denotes significance differences between groups (*p<0.05; **p<0.01; Mann-Whitney test). N.S. denotes no significant difference.

Figure 2. **Glutamate photolysis inhibits presynaptic LTP and augments presynaptic LTD.** (**A**) Left, an image of a CA1 neuronal dendrite loaded with Oregon Green Bapta-1 Ca^{2+} dye. A stimulating electrode (SE; green) was placed close to the dendrite in order to activate spines within the vicinity (scale bar: 2µm). A spine responsive to stimulation was located and then targeted for glutamate photolysis (yellow spot). An example of an uncaging-evoked synaptic potential is shown above the imaged spine (scale bar: 1mv by 100ms). During stimulation and photolysis, evoked Ca^{2+} transients were rapidly imaged by restricting laser scanning to a line across the spine head and underlying dendrite (broken line). Right, samples of these Ca^{2+} transients in both the spine (labelled S) and dendritic (labelled D) are shown. Below each line scan image are traces quantifying the fluorescence change (%ΔF/F) for the spine (red trace; raw) and dendrite (purple trace; raw). (**B,C**) Samples of 10 superimposed Ca^{2+} traces evoked in imaged spines (white scale bar: 2µm)

by paired pulse stimulation (P1 and P2 were delivered 70ms apart and are represented by vertical broken lines); red traces depict successful release events to the first (P1) of the two pulses. Ca^{2+} traces are shown during baseline and 25-30 minutes following paired or unpaired stimulation, delivered in either the absence or presence of glutamate photolysis (yellow circle). Transmitter release probability (Pr) was calculated as the proportion of total stimulation trials in which the first pulse (P1) resulted in a successful release event. (**D,E**) The final P_r measured 25-30 minutes following stimulation is plotted against the initial P_r measured at baseline for each imaged synapse. The broken diagonal line represents the expected trend if P_r was unchanged. The post-photolysis control group consists of 5 synapses from the photolysis group that underwent a second round of paired stimulation but in the absence of glutamate photolysis. (**H,I**) EPSP is plotted against time. The point at which stimulation was delivered is denoted by the black arrow. (**J**) Average change in EPSP slope. (**K**) Average change in Pr. Error bars represent S.E.M. (n=9-14 per condition). Asterisks denotes significance differences between groups (*p<0.05; **p<0.01; Mann-Whitney test). N.S. denotes no significant difference.

Figure 3. Induction of presynaptic LTP in glutamate receptor blockade. (**A**) Experimental setup. CA1 neurons in cultures hippocampal slices were recorded using high resistance patch electrodes (18-25MΩ). EPSPs were recorded from two independent Schaffer-collateral pathways. LTP was induced in a full glutamate receptor blockade (AP5, NBQX, MCPG, and LY341495) by paired stimulation. An example of the pairing protocol is shown. Only one pathway (black box) was active during paired stimulation, the other pathway served as a control (white boxes). (**B**) Average fold change in the EPSP slope is plotted against time for both the control and paired pathways (n=12). Sample EPSP traces shown are averages of 10 traces from the paired (solid line) and control (broken line) pathway taken at four time points (1-4) from a single experiment (scale bar: 4.0mV by 40ms for paired pathway EPSP, 4.9mV by 40ms for control pathway EPSP). Stimulation artifacts have been removed for clarity. (**C**) Average fold change in EPSP slope is plotted for control experiments in which glutamate receptor antagonists were applied alone, in the absence

of paired stimulation (drugs only group). Note that drug washout was incomplete. Group data and averages plotted for fold changes in (**D**) EPSP slope, (**E**) CV^{-2} and (**F**) paired pulse ratio (PPR) across experiments as measured 30 minutes following paired stimulation and drug washout. EPSP slope was higher in the paired pathway than in the control pathway, and was associated with an increase in CV^{-2} and a decrease in PPR, suggesting that LTP had been induced in the paired pathway, and had a presynaptic locus of expression. Error bars represent S.E.M. (n=5-7 per condition). Asterisks denotes significance differences between groups (*p<0.05; Wilcoxon matched pairs test or Mann-Whitney test). N.S. denotes no significant differences between groups.

Figure 4. **LTP induction in glutamate receptor blockade is associated with an increase in transmitter release probability (Pr) at single CA3-CA1 synapses.** (**Ai**) Example experiment. Left, an image of a CA1 neuronal dendrite loaded with Oregon Green Bapta-1 Ca^{2+}-sensitive dye with a stimulating electrode (SE) placed close to the dendrite in order to activate synapses within the vicinity (scale bar: 5µm). Example of Ca^{2+} transients were evoked by two stimulation pulses (P1 and P2) delivered 70ms apart are shown in spine head (S) and underlying dendrite (D). Below the line scan are raw (grey) and smoothened (colored) traces quantifying fluorescence changes (ΔF/F) in the spine (black trace) and dendrite (purple trace). (**Aii**) The peak ΔF/F in the spine head following the first of the two stimulation pulses (P1) is plotted across 30 paired pulse stimulation trials given at baseline and 30 minutes following paired stimulation, which was delivered in full glutamate receptor blockade (AP5, NBQX, MCGP, LY341495). Red squares denote fluorescent increases above noise. Smoothened Ca^{2+} traces from the last 10 trials are shown above each graph. P_r was calculated as the proportion of total stimulation trials in which the first pulse (P1) resulted in a fluorescent increase above noise. (**B**) Group data. For each experiment, the imaged synapse's initial P_r is plotted against its final P_r, calculated 30 minutes following one of five different stimulation paradigms. Only causal pairing of pre- and post- synaptic activity generated increases in P_r (**C**) Average change in P_r across experimental conditions for data in (B). Error bars represent S.E.M. (n=6-10 per condition).

Asterisks denotes significance differences between the first group in the graph (**p<0.01; Mann-Whitney test).

Figure 5. Postsynaptic depolarization increases transmitter release probability (Pr) by promoting dendritic release of nitric oxide in a manner dependent on L-type voltage-gated Ca^{2+} channels (L-VGCCs). (**A**) Average change in P_r. Paired stimulation was delivered under control conditions, following treatment with the L-VGCC antagonist nitrendipine, or following either the bath or intracellular application of the NO scavenger cPTIO. (**B**) Images of CA1 apical dendrites loaded with NO-sensitive fluorescent dye (DAF-FM), prior to and following K^+ mediated depolarization (scale bar: 5µm) in control conditions, or in the presence of nitrendipine, cPTIO, or the NO synthesis inhibitor L-NAME. (**C**) Average K^+ induced fluorescence change (ΔF/F) of DAF-FM in apical dendrites. (**D**) Samples of 10 superimposed Ca^{2+} traces evoked in imaged spines (white scale bar: 1µm) by paired pulse stimulation (broken vertical lines show 2 stimuli delivered 70ms apart); red traces depict successful release events to the first of the two pulses. Samples are taken from baseline and 25-30 minutes following a stimulation paradigm. The paradigm consisted of delivering presynaptic stimuli either (top) 10ms before or (bottom) 10ms after NO photolysis at the synapse (yellow circle); photolysis occurred in glutamate receptor blockade and in the absence of postsynaptic depolarization. P_r was calculated as the proportion of total stimulation trials in which the first pulse resulted in a successful release event. In some experiments NO photolysis was conducted in cPTIO. (**E**) Final P_r measured 25-30 minutes following the stimulation paradigm is plotted against the initial P_r for each synapse. The broken diagonal line represents the expected trend if P_r was unchanged. (**F**) Average change in Pr. Error bars represent S.E.M. (n=5-13 per condition). Asterisks denote significant differences from the control group (*p<0.05; **p<0.01; Mann-Whitney test).

Figure 6. Glutamate release decreases transmitter release probability (P_r) via presynaptic NMDAR signalling. (**A**) Samples of 10 superimposed Ca^{2+} traces evoked in imaged spines (white scale bar: 1µm) by paired pulse stimulation (2 stimuli delivered 70ms

apart; represented by the vertical broken lines); red traces depict successful release events to the first of the two pulses. P_r was calculated as the proportion of total stimulation trials in which the first pulse resulted in a successful release event. For each spine, sample Ca^{2+} traces are shown during baseline and 25-30 minutes following paired stimulation. Experiments were also conducted with unpaired stimulation, in which presynaptic activity was delivered in the absence of postsynaptic depolarization. **(B, D)** Paired or unpaired stimulation was delivered in control conditions or following: full glutamate receptor blockade (AP5, NBQX, MCPG, and LY341495), bath application of AP5, MK-801, or intracellular application of MK-801.For each experiment, the final P_r measured 25-30 minutes following (B) paired or (E) unpaired stimulation is plotted against the initial P_r measured at baseline. Red trendlines have been fitted to control data. The broken diagonal line represents the expected trend if P_r was unchanged. **(C,E)** Average change in Pr. Error bars represent S.E.M. (n=9-18 per condition). Asterisks denote significant differences from control data (**p<0.01; Mann-Whitney test). N.S. denotes no significant difference from control data unless otherwise specified.

Figure 7. Inhibition of presynaptic NMDARs rescues the effects of glutamate photolysis on presynaptic plasticity. (A, C) Photolysis experiments conducted in Figure 1 are shown, in which paired or unpaired stimulation was delivered in the presence or absence of glutamate photolysis. Experiments were repeated following either the bath or intracellular application of MK-801. For each experiment, the final P_r measured 25-30 minutes following (A) paired or (C) unpaired stimulation is plotted against the initial P_r measured at baseline. The broken diagonal line represents the expected trend if P_r was unchanged. Bath, but not intracellular, application of MK-801 prevents (A) photolysis-induced inhibition of LTP and (C) photolysis-induced augmentation of LTD, suggesting that the effects of photolysis are mediated by presynaptic NMDAR signalling. **(B,D)** Average change in Pr. Error bars represent S.E.M. (n=7-13 per condition). Asterisks denote significant differences from control data (*p<0.05 or **p<0.01; Mann-Whitney test), unless a

pairwise comparison is specified. N.S. denotes no significant difference from control data unless otherwise specified.

Figure 8. A simple mathematical framework predicts activity-dependent changes in P_r
(A) Experimental model of presynaptic plasticity. Changes in P_r at active presynaptic terminals are determined by two opponent processes. 1) Increases in P_r are driven by strong postsynaptic depolarization, which triggers the release of nitric oxide (NO) from neuronal dendrites. NO synthesis is dependent on NO synthase (NOS), activation of which is triggered by Ca^{2+} influx through L-type voltage-gated Ca^{2+} channels (L-VGCC). Importantly, NO drives an increase in P_r, but only at presynaptic terminals whose activity precedes its release. The detection of such an event requires an effector (Δt) that is sensitive to the relative timings of NO release and presynaptic activity. 2) Decreases in P_r are driven by glutamate release ([glu]), via presynaptic NMDA receptor (NMDAR) signalling. Net changes in P_r depend on the strengths of both processes, and therefore on the levels of postsynaptic depolarization and glutamate release that accompany presynaptic activity. **(B)** Proposed mathematical framework of presynaptic plasticity, in which $\Delta P_r = \eta (P_{depol}-P_{glu})$. P_{depol} is the probability that presynaptic activity is casually accompanied by strong postsynaptic depolarization during plasticity induction. P_{glu} is the probability that glutamate was released at the synapse during plasticity induction. η is a constant defined as the learning rate, which was determined to be 0.35 to achieve the best fit. **(C)** Data (n=216 synapses) were divided into 6 categories based on experimental manipulations during plasticity induction in which 60 presynaptic stimuli were delivered at 5Hz. These manipulations include all experimental conditions in which the effects of postsynaptic depolarization were present or absent, whether glutamate photolysis (yellow dot) was present or absent, and whether presynaptic NMDAR blockade (red cross) was present or absent. These categories, along with the associated value of P_{depol}, P_{glu}, and ΔP_r, are summarized in table form. Where P_{glu} did not take the value of 0 or 1, it was calculated using the following formula: $P_{glu} = 0.475*\text{basal } P_r + 0.2175$; see Supplemental Figure 4 for further details. **(D)** For each category, the initial P_r is plotted against final P_r for all

synapses within the category. A line of best fit for the data is shown in grey. The model's predictions are shown in red. The model's predictions are in close agreement with the lines of best fit, except for the fourth category, in which presynaptic stimulation is delivered in the presence of glutamate photolysis but in the absence of postsynaptic depolarization. **(E)** For each condition, the variance explained by the model is compared to that explained by the line of best fit. No significant differences (N.S.) are found across categories and overall. The model achieved a substantially better (i.e. lower) Bayesian Information Criterion (BIC) than the lines of best fit ($BIC_{\text{line of best fit}} - BIC_{\text{model}} = 34.97$). This was also the case when categories having similar trends were combined (category 1 and 6) to minimize the free parameters used by the lines of best fit from 12 to 10 ($BIC_{\text{line of best fit}} - BIC_{\text{model}} = 24.25$). Thus, the model represents a parsimonious framework that captures the general trend of the data despite only having a single free parameter (η, the learning rate), as compared to a total of 12 free parameters collectively used by the lines of best fits (2 free parameters per line, the slope and the intercept).

Supplemental Figure 1. Induction of presynaptic LTP under glutamate receptor blockade in acute hippocampal slices. EPSPs were recorded from two independent Schaffer-collateral pathways in acute hippocampal slices. LTP was induced by pairing each of 60 presynaptic stimuli, delivered at 5Hz in glutamate receptor blockade (AP5, NBQX, MCPG, LY341495), with postsynaptic depolarization in the form of a complex spike (see Figure 1A for example). Only the paired pathway was active during paired stimulation. (**A**) Fold change in the EPSP slope is plotted against time for both control and paired pathways (n=6). Paired stimulation was delivered in glutamate receptor blockade alone, or in the additional presence of the L-VGCC blocker nitrendipine, or the NO scavenger cPTIO. (**B**) Average fold change in EPSP slope in the paired pathway 30 minutes following paired stimulation and drug washout; values are normalized to the EPSP slope recorded in the control pathway. (**C**) Average fold change in CV^{-2} in the paired pathway; values are normalized to the EPSP slope recorded in the control pathway. (**D**) Average change in paired pulse ratio (PPR) in the paired pathway. Paired stimulation elicited potentiation of

the EPSP slope, and was accompanied by an increase in CV^{-2} and a decrease in PPR, suggesting that LTP induction had a presynaptic component of expression. No such changes were observed when pairing occurred in the presence of nitrendipine or cPTIO. Error bars represent S.E.M. (n=5-6 per condition). Asterisks denote significant differences from the first group in the graphs (*p<0.05; **p<0.01; Mann-Whitney test).

Supplemental Figure 2. Data summary for acute slice experiments. Same experiment as Figure S1, but data are individually plotted for both the paired and control pathways, without normalization. Fold change in the EPSP slope, fold change in CV^{-2}, and change in paired pulse ratio (PPR) are plotted for experiments involving (**A**) paired stimulation in the presence of glutamate receptor antagonists, (**B**) paired stimulation in the presence of glutamate receptor antagonists and the L-VGCC antagonist nitrendipine, or (**C**) paired stimulation in the presence of glutamate receptor antagonists and the NO scavenger cPTIO. The presence of nitrendipine and cPTIO prevented pairing-induced increases in EPSP slope, increases in CV^{-2}, and decreases in PPR. Asterisks denotes significance differences between groups (*p<0.05; Wilcoxon-matched pairs test). N.S. denotes no significant differences between groups.

Supplemental Figure 3. **Spine Ca^{2+} transients in NMDA receptor blockade are mediated by voltage-gated Ca^{2+} channels, and can be used to accurately measure Pr.** (**A**) NMDA receptor (NMDAR) blockade does not impede measurement of transmitter release probability (Pr). Samples of 10 superimposed Ca^{2+} traces evoked in imaged spines (white scale bar: 1µm) by paired pulse stimulation (broken vertical lines show 2 stimuli delivered 70ms apart); red traces depict successful release events to the first of the two pulses. Pr was calculated as the proportion of total stimulation trials in which the first pulse resulted in a Ca^{2+} response in the dendritic spine. (i,ii) For two imaged spines, sample Ca^{2+} traces are shown prior to and following bath application of AP5. AP5 abolished Ca^{2+} transients ($\%\Delta F/F < 20\%$) in only one of the two spines. (**B**) For each synapse imaged, the Pr measured under basal conditions is plotted against the Pr measured during bath

application of AP5. The broken diagonal line represents the expected trend if Pr is unchanged. For about 50% of synapses, a significant Ca^{2+} transient remained in AP5 (black boxes; %ΔF/F > 20%); at these sites, Pr measured under basal conditions was unchanged by AP5. (**C**) Group data depicted no significant difference between Pr measured under basal conditions and in AP5 for synapses for which an AP5-insensitive Ca^{2+} transient could be detected (%ΔF/F $\geq$ 20%). (**D**) Residual Ca^{2+} influx in AP5 is mediated by voltage-gated Ca^{2+} channels. Images of sample Ca^{2+} responses evoked by stimulation or glutamate photolysis at a single spine under various pharmacological manipulations. Below each image are traces quantifying the change in fluorescence intensity of the Ca^{2+} response (%ΔF/F). At the spine shown, AP5 reduced, but did not abolish, Ca^{2+} responses evoked by stimulation. Inhibition of voltage-gated calcium channels by Ni^{2+} (100μM) and Cd^{2+}(100μM) abolished the AP5-insensitive component of the Ca^{2+} transient; since Ni^{2+} and Cd^{2+} inhibit transmitter release, glutamate release was simulated via photolysis under these conditions. (**E**) Average peak amplitude of evoked Ca^{2+} responses (ΔF/F) across experimental conditions (n=5-12/condition). Ca^{2+} responses evoked by glutamate photolysis did not significantly differ from those evoked by electrical stimulation, and was significantly reduced by Ni^{2+} and Cd^{2+} application. (**F**) Intracellular application of MK-801 effectively blocks NMDARs. Images of sample Ca^{2+} responses evoked by single presynaptic stimuli with intracellular application of MK-801 and following the addition of AP5. Below each image are traces quantifying the change in fluorescence intensity of the Ca^{2+} response (%ΔF/F). (**G**) Average peak Ca^{2+} fluorescence amplitude (ΔF/F) evoked by electrical stimulation following either intracellular application of MK-801 or bath application of AP5; response amplitudes recorded in AP5 and MK801 do not differ, and are significantly lower than those recorded in control conditions, in which NMDARs are not blocked. Scale bars: 1μm. Error bars represent S.E.M. (n=5-12 per condition). Asterisks denote significant differences (**p<0.01; Mann-Whitney or Wilcoxon-matched pairs tests). N.S. denotes no significant difference.

Supplemental Figure 4. Estimating glutamate release probability during 5Hz theta stimulation. Ca^{2+} imaging was used to monitor glutamate release at single synapses during a presynaptic stimulus train consisting of 60 stimuli delivered at 5Hz. The probability of glutamate release during the train (P_{glu}) was calculated as the number of release events divided by the number of presynaptic pulses (i.e. 60). For each synapse, P_{glu} is plotted against basal $P_{r.}$ The data was fit with a linear regression line to derive a basis by which to estimate P_{glu} given basal P_r. The regression line was significant (n=24 synapses; $p<0.01$).

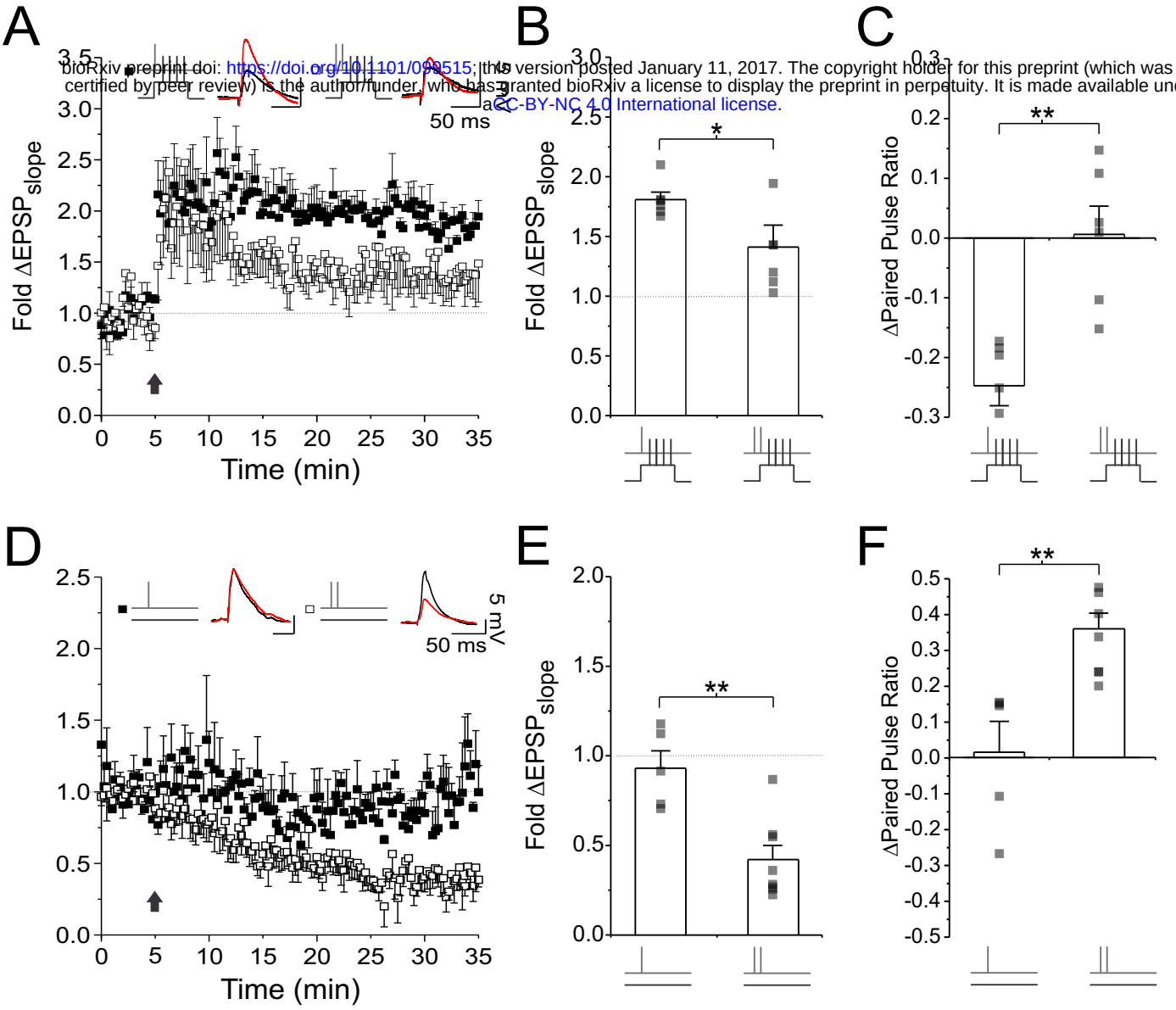

Figure 1

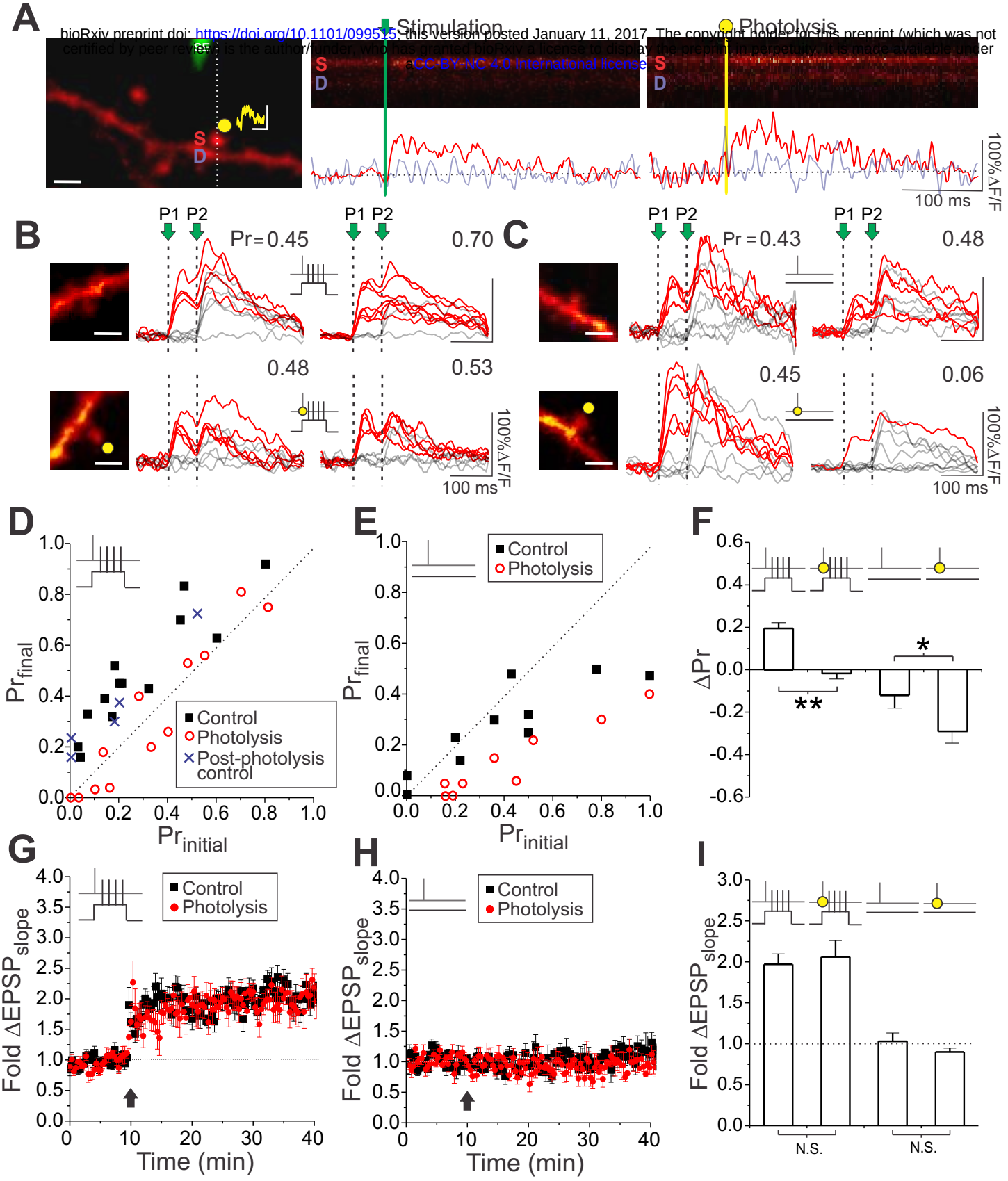

Figure 2

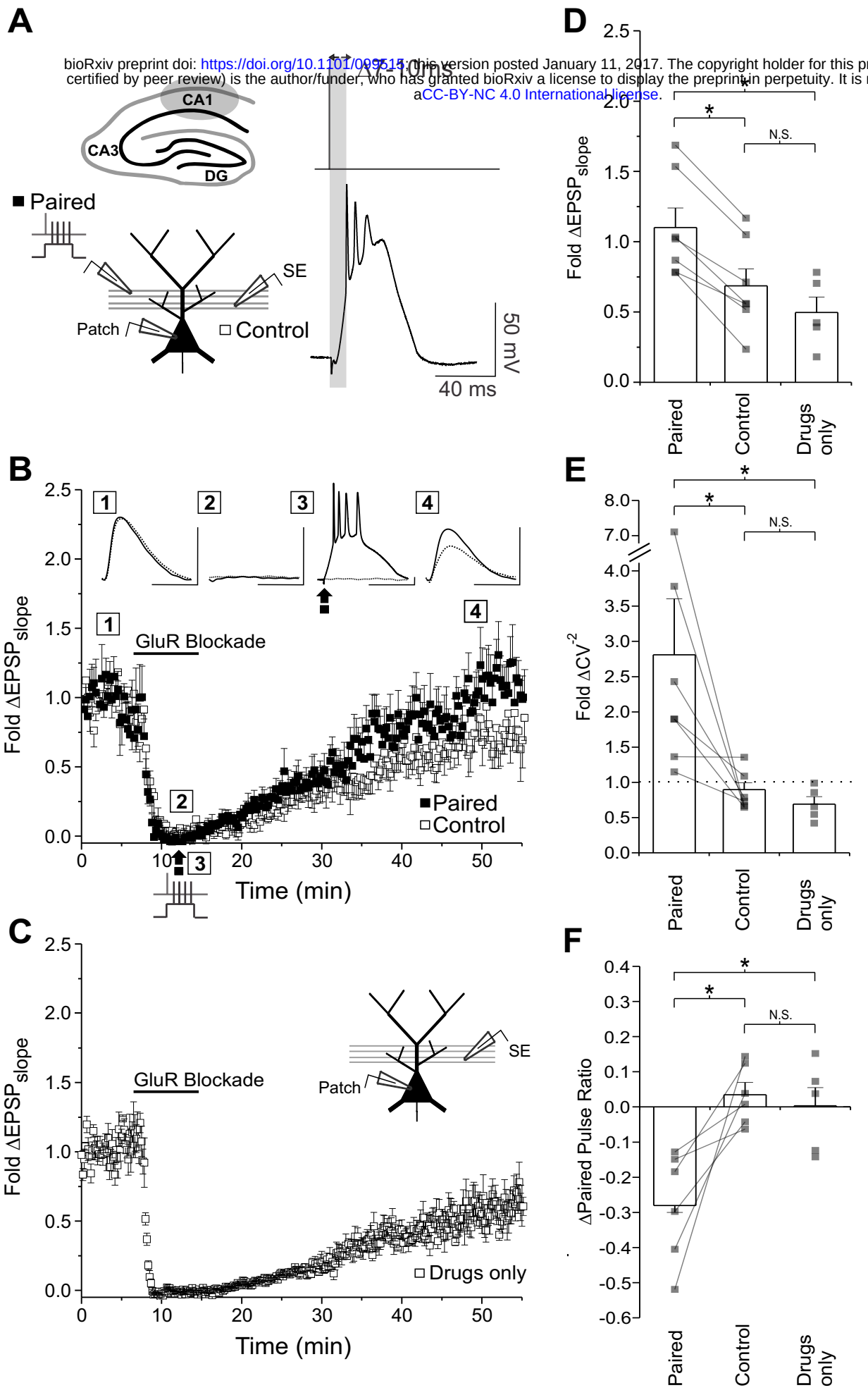

Figure 3

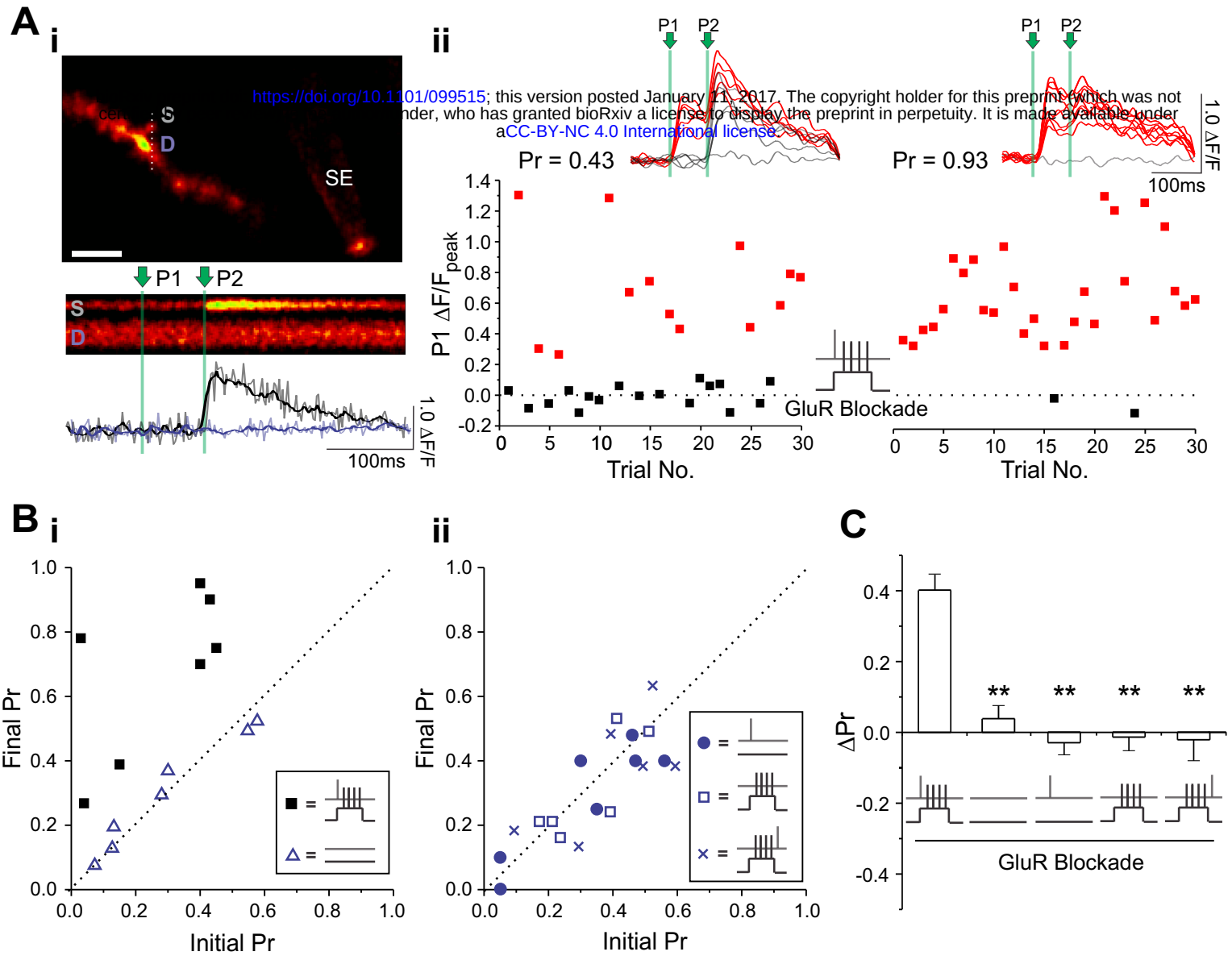

Figure 4

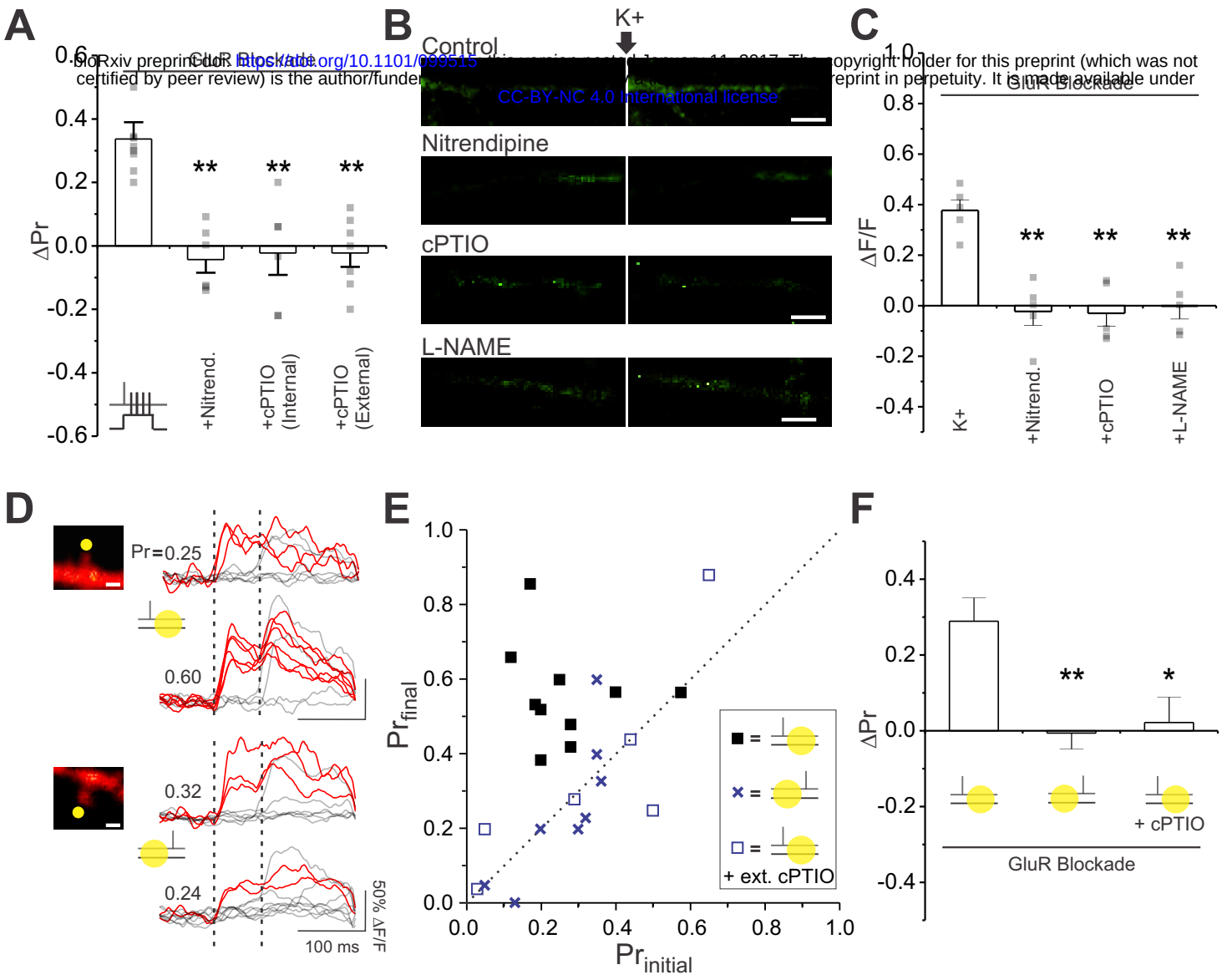

Figure 5

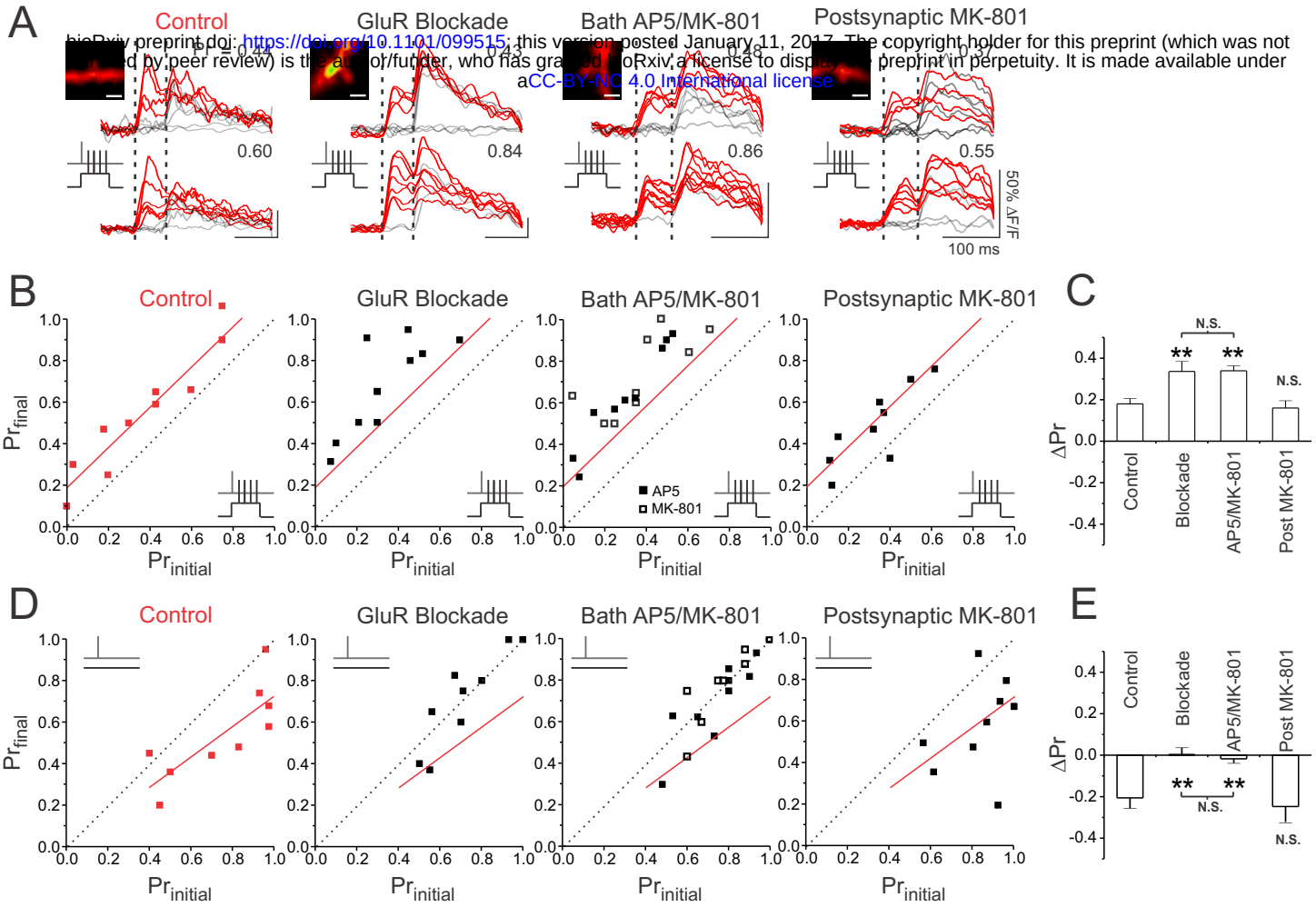

Figure 6

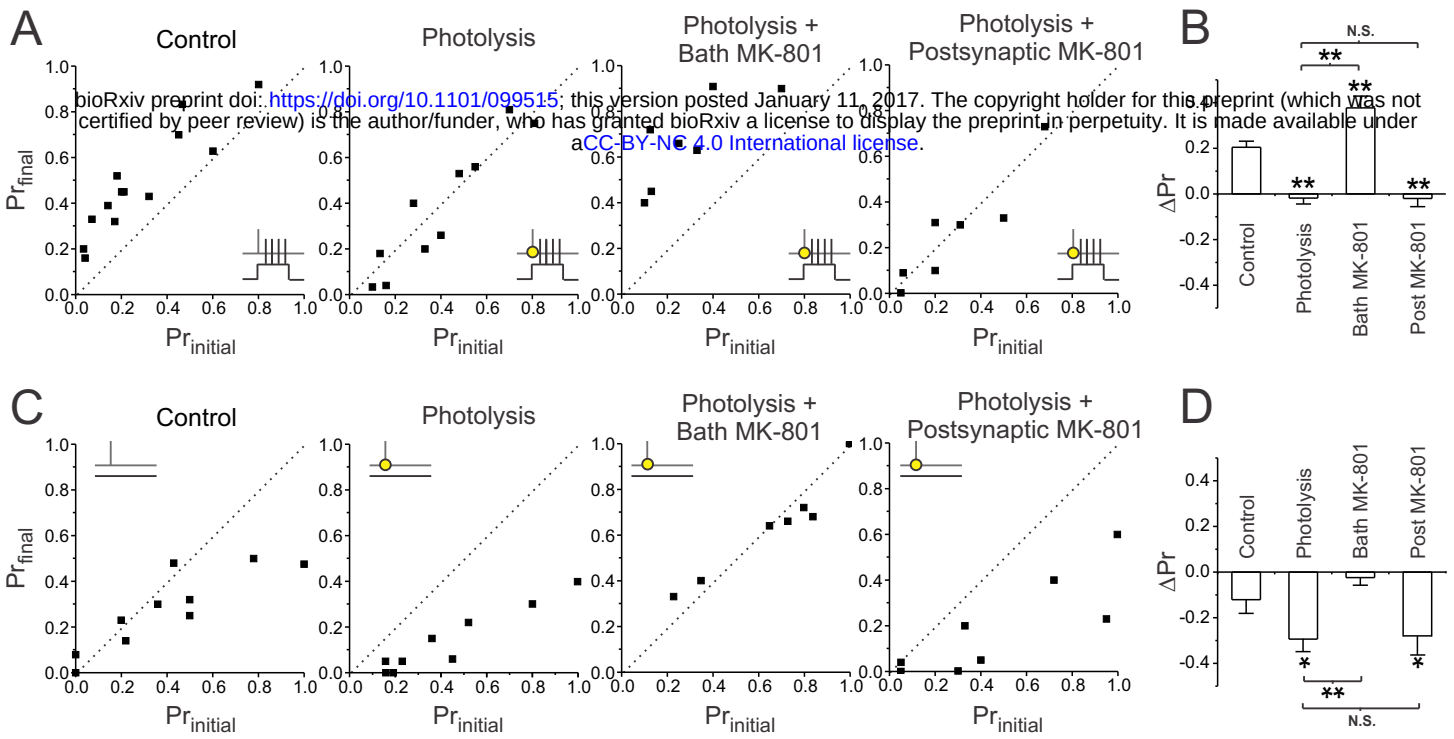

Figure 7

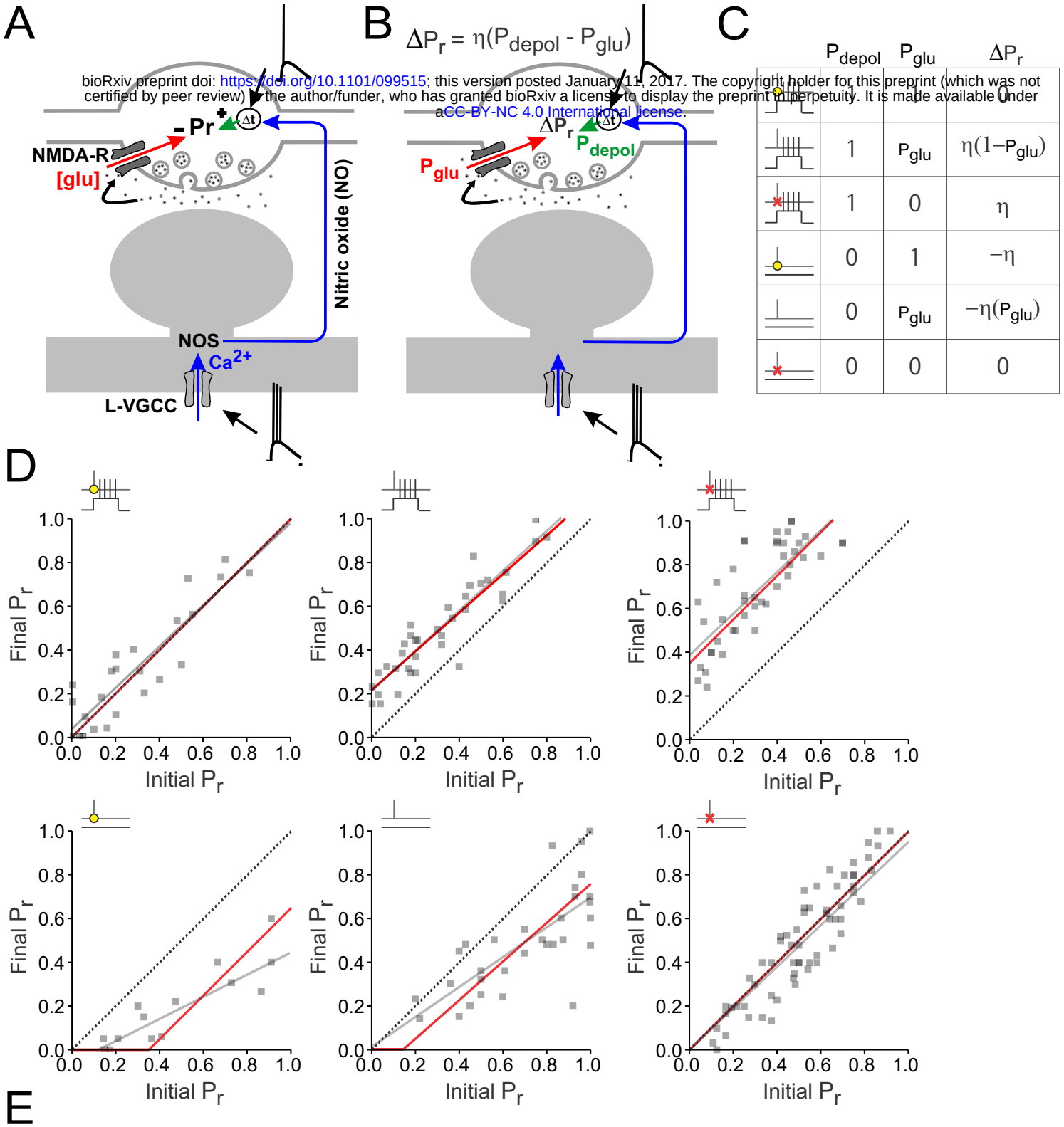

Figure 8

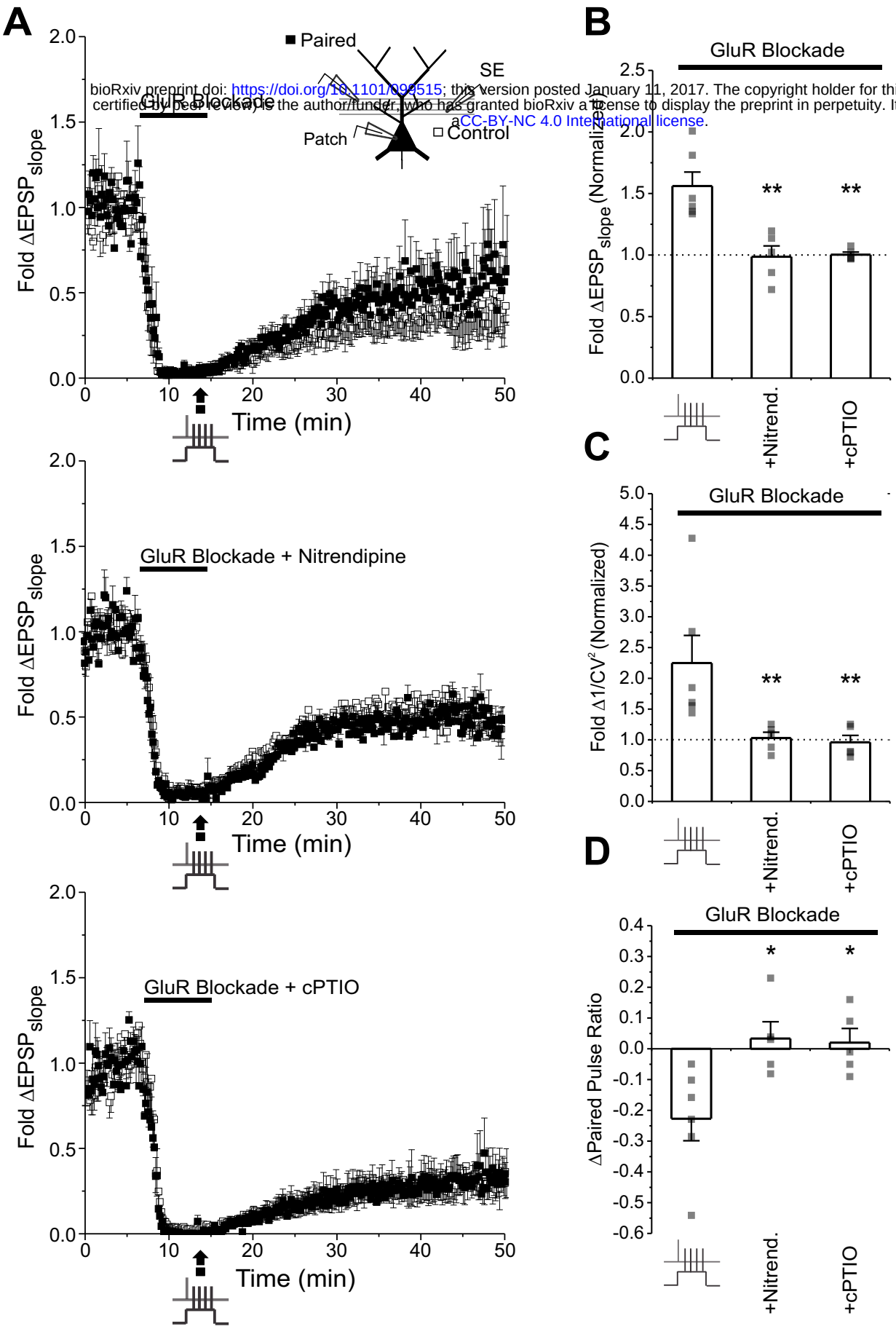

Supplemental Figure 1

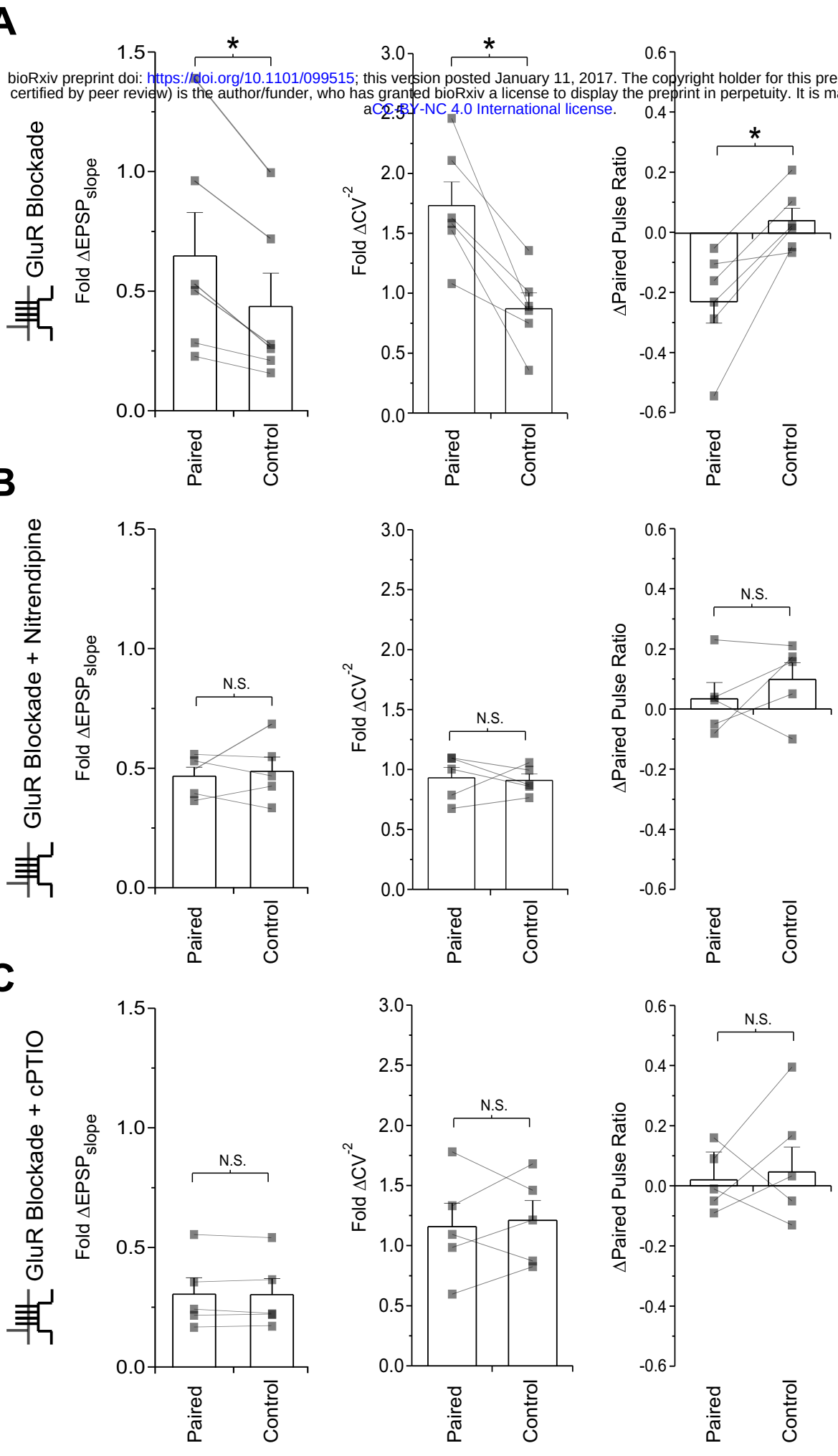

Supplemental Figure 2

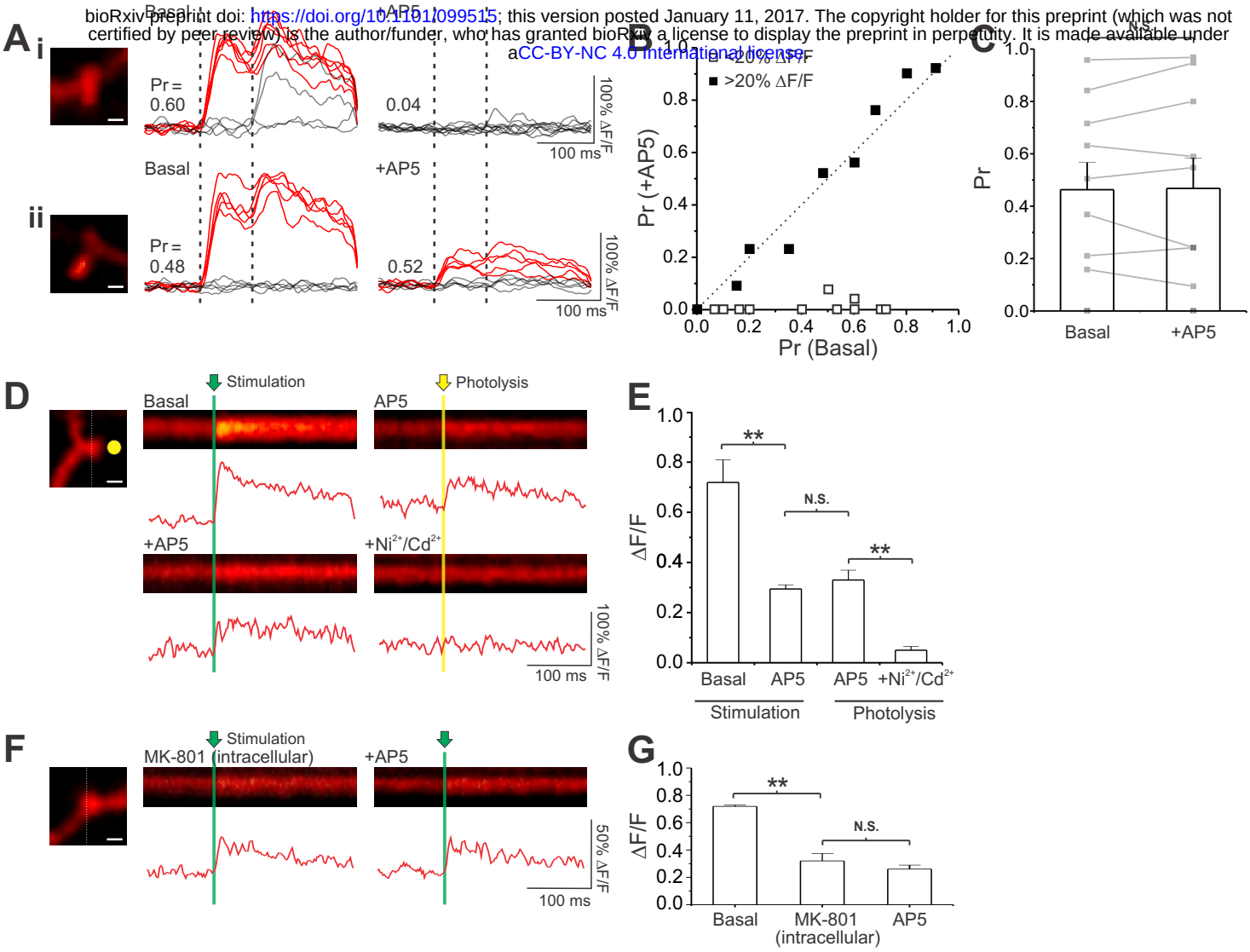

Supplemental Figure 3

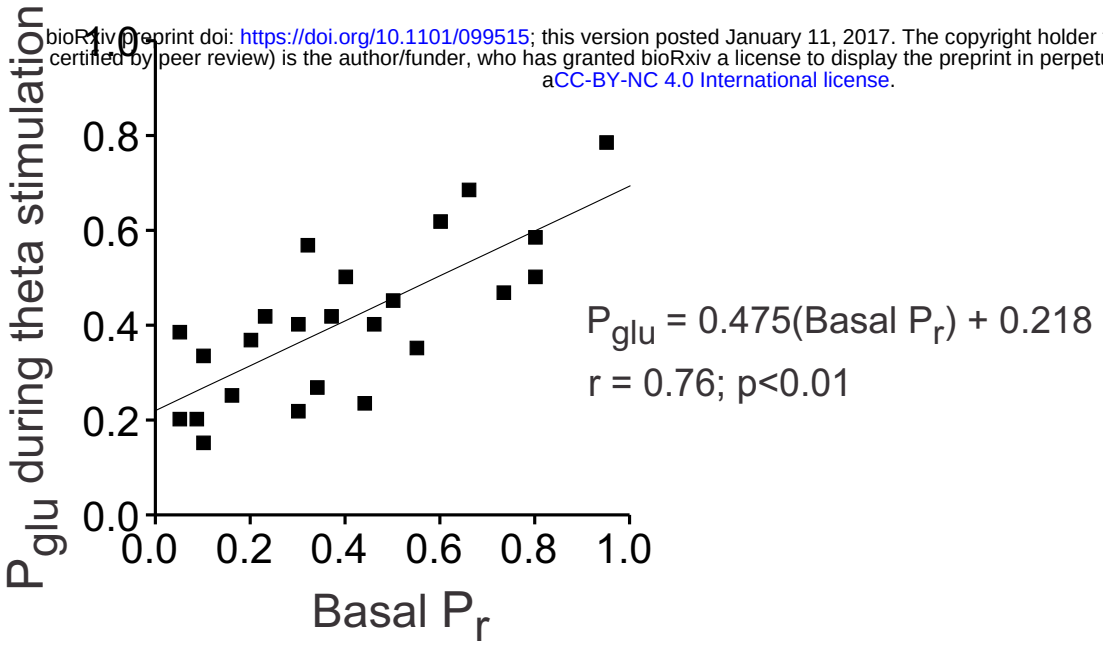

Supplemental Figure 4